

A Ruthenium(II) Complex Containing a Redox-Active Semiquinonate Ligand as Potential Chemotherapeutic Agent: From Synthesis to *in vivo* Studies

Anna Notaro,^{a,#} Angelo Frei,^{b,#} Riccardo Rubbiani,^{b,#} Marta Jakubaszek,^{a,e} Uttara Basu,^a Severin Koch,^b Cristina Mari,^b Mazzarine Dotou,^a Olivier Blacque,^b Jérémie Gouyon,^c Fethi Bedioui,^c Nils Rotthowe,^d Rainer F. Winter,^d Bruno Goud,^e Stefano Ferrari,^f Mickaël Tharaud,^g Martina Řezáčová,^h Jana Humajová,ⁱ Pavel Tomšík,^h and Gilles Gasser^{a,}*

- ^a Chimie ParisTech, PSL University, CNRS, Institute of Chemistry for Life and Health Sciences, Laboratory for Inorganic Chemical Biology, F-75005 Paris, France.
- ^b Department of Chemistry, University of Zurich, Winterthurerstrasse 190, 8057 Zurich, Switzerland.
- ^c Chimie ParisTech, PSL University, CNRS, Institute of Chemistry for Life and Health Sciences, Team Synthèse, Electrochimie, Imagerie et Systèmes Analytiques pour le Diagnostic, F-75005 Paris, France.
- ^d Department of Chemistry, University of Konstanz, Universitätsstrasse 10, D-78457 Konstanz, Germany.
- ^e Institut Curie, PSL University, CNRS UMR 144, Paris, France.
- ^f Institute of Molecular Cancer Research, University of Zurich, Zurich, Switzerland.
- ^g Université de Paris, Institut de physique du globe de Paris, CNRS, F-75005 Paris, France.
- ^h Department of Medical Biochemistry, Faculty of Medicine in Hradec Kralove, Charles University, Czech Republic.
- ⁱ Department of Medical Biochemistry, Faculty of Medicine in Hradec Kralove, Charles University, Czech Republic.

ⁱ Department of Medical Biochemistry, Faculty of Medicine in Prague, Czech Republic.

[#] these authors have contributed equally to the work

* Corresponding author: E-mail: gilles.gasser@chimeparistech.psl.eu; WWW: www.gassergroup.com; Phone: +33 1 44 27 56 02

ORCID Number

Anna Notaro: 0000-0003-0148-1160

Angelo Frei: 0000-0001-6169-2491

Marta Jakubaszek: 0000-0001-7590-2330

Uttara Basu: 0000-0002-0509-2421

Mazzarine Dotou: 0000-0001-8781-6763

Olivier Blacque: 0000-0001-9857-4042

Fethi Bedioui: 0000-0002-0063-4412

Bruno Goud: 0000-0003-1227-4159

Stefano Ferrari: 0000-0002-6607-215X

Martina Řezáčová 0000-0001-5370-2290

Jana Humajová (Mattová) 0000-0001-8099-6781

Pavel Tomšík 0000-0002-4366-075X

Gilles Gasser: 0000-0002-4244-5097

Keywords: Bioinorganic Chemistry, Cancer, DNA, Medicinal Inorganic Chemistry, Ruthenium.

Abstract

Chemotherapy remains one of the dominant treatments to cure cancer. However, due to the many inherent drawbacks, there is a surge for new chemotherapeutic drugs. More specifically, the discovery of new drug candidates able to overcome severe side effects, the occurrence of resistance and the inefficacy toward metastatic tumours is highly desirable. In this work, we designed a new chemotherapeutic drug candidate against cancer, namely [Ru(DIP)₂(sq)]PF₆ (**Ru-sq**) (DIP = 4,7-diphenyl-1,10-phenanthroline; sq = semiquinonate ligand). The aim was to combine the great potential expressed by Ru(II) polypyridyl complexes and the singular redox and biological properties associated to the catecholate moiety. Several pieces of experimental evidence (e.g., X-ray crystallography, electron paramagnetic resonance, electrochemistry) demonstrate that the semiquinonate is the preferred oxidation state of the dioxo ligand in this complex. The biological activity of **Ru-sq** was then scrutinised *in vitro* and *in vivo*, and the results highlight the tremendous potential of this complex as a chemotherapeutic agent against cancer. **Ru-sq** was notably found have a much higher cytotoxic activity than cisplatin on several cell lines (i.e. in the nanomolar range), and, contrary to cisplatin, to have mitochondrial dysfunction as one of its modes of action. The multicellular targets of **Ru-sq** could potentially be the key to overcome one of the main drawbacks of cisplatin i.e. the occurrence of resistance. Moreover, **Ru-sq** exhibited impressive activity on Multi Cellular Tumour Spheroids (MCTS) model, leading to a growth inhibition of the tumour even 13 days after treatment (20 μM). Very importantly, using two different *in vivo* models, it could be demonstrated that this compound is extremely well-tolerated by mice and has a very promising activity, curing, in some cases, tumour-bearing mice.

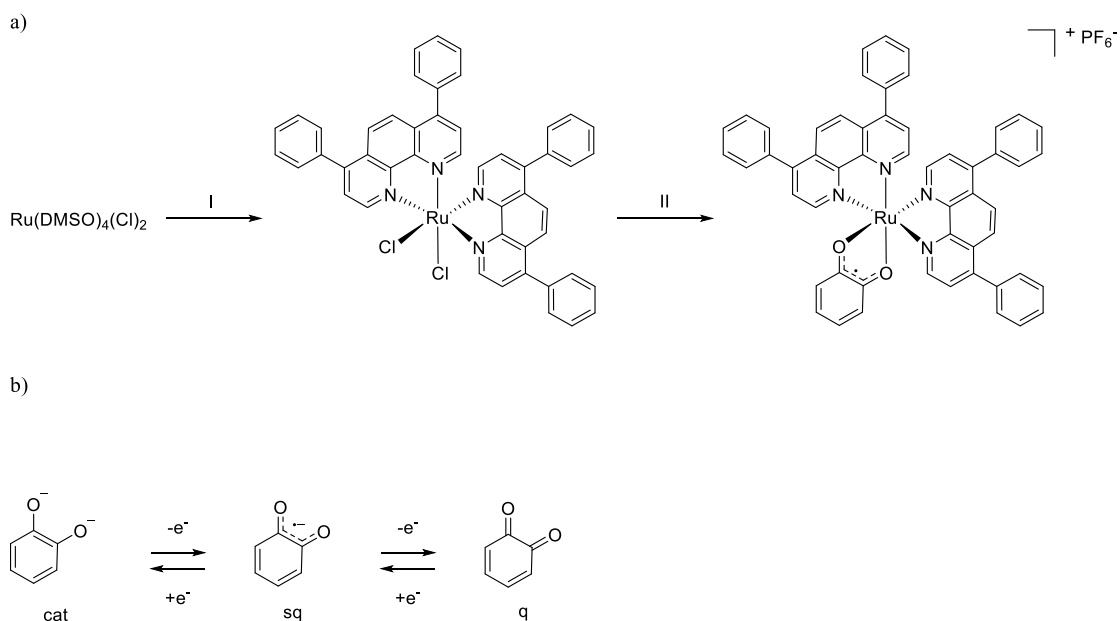
Introduction

In the last decades, the search for new chemotherapeutic agents against cancer has challenged scientists worldwide. Chemotherapy, together with surgery, radiotherapy and immunotherapy, is used in the so-called combination therapy to treat cancer.¹ The goal of this combination is to overcome the drawbacks of each singular treatment to afford the best chances of survival for the patients.¹ Cisplatin is one of the most common chemotherapeutic agents utilized against cancer. However, its severe side effects are limiting its clinical use.²⁻⁶ Therefore, many other platinum-based drug candidates have been investigated over the last 40 years leading to the worldwide clinical approval of carboplatin and oxaliplatin.^{7,8} On the basis of these groundbreaking discoveries and the observed occurrence of resistance with platinum treatment, a large number of metal complexes based on other metals than platinum have been examined.⁹⁻¹⁶ In this field, ruthenium complexes play a central role due to their inherent advantages (i.e. multiple stable oxidation states, higher selectivity towards cancer cells, etc.).¹⁷⁻²⁰ KP-1019, KP-1339 and NAMI-A are, to date, the only three Ru complexes to have reached clinical trial as anticancer agents. Their mechanism of action involves ligand exchange, resembling therefore the one of cisplatin.²¹⁻²⁴ Of note, TLD1433, an inert Ru(II) polypyridyl complex, has just completed phase I clinical trial as a photodynamic therapy photosensitizer against bladder cancer.²⁵ Ruthenium complexes find applications in different fields of medicinal chemistry against cancer, exploiting a large variety of mechanisms of action.²⁶⁻³¹ A very promising class of ruthenium complexes are the coordinatively saturated and substitutionally inert ruthenium polypyridyl complexes. These compounds have been intensely investigated over the last years and several applications as potential chemotherapeutic agents have been unearthed.²⁶ At first, most of the bio-activity of these compounds was associated

with interactions with DNA.^{32–35} However, over the years, many other modes of action were identified, such as the trigger of mitochondria dysfunction,^{36–38} Topoisomerases I and II inhibition,^{39,40} modification of cell membranes⁴¹ and others.²⁶

Due to the great opportunities offered by this class of Ru compounds, in this work, we designed a new Ru polypyridyl complex, namely [Ru(DIP)₂(sq)](PF₆) (**Ru-sq**, Scheme 1a) where DIP is 4,7-diphenyl-1,10-phenanthroline and sq is a semiquinonate ligand, which was found to be a very interesting anticancer drug candidate. Semiquinonate is a so-called ‘non-innocent’ ligand as its electrochemical properties strongly resemble that of the metal center.⁴² Semiquinonate is the oxidised form of catechol, a well-known dioxolane ligand, which can exist in three redox forms, namely catecholate (cat), semiquinonate (sq) and quinone (q) (Scheme 1b).⁴³ Catecholate and its oxidation products have already been intensively investigated as ligands.^{44,45} However, the focus of these studies has mostly been on the unique electronic/redox properties of metal complexes containing such ‘non-innocent’ dioxolane ligands.^{46–49} Catechols are also known as pan-assay interference compounds (PAINS) due to their redox and chelating properties.⁵⁰ Nevertheless, catecholate and its derivatives have also shown potential in different fields of biological interest,^{51–55} such as cancer chemoprevention,⁵³ antifungal activity⁵⁴ and the inhibition of the spontaneous A β fibril formation,⁵⁵ which is a key target for the treatment of Alzheimer’s disease. Worthy of note, vanadium compounds carrying catechol-like ligands have been investigated by Crans and co-workers.^{56,57} During these studies, particularly potent cytotoxic vanadium (V) catecholate complexes toward bone cancer cells were unveiled.⁵⁶ The cytotoxicity on glial cells of [Ru^{III}(NH₃)₄(catecholate)]⁺ was also investigated in 2007 by Almeida and co-workers.⁵² In this case, the catechol was found to be more cytotoxic than the Ru(III) complex itself with an EC₅₀ of 0.342 mM against rat astrocytes and 0.568 mM against human

glioblastoma GL-15 cell line, while the $[\text{Ru}^{\text{III}}(\text{NH}_3)_4(\text{catecholate})]^+$ complex had $\text{EC}_{50} = 1.380 \text{ mM}$ and $\text{EC}_{50} = 2.6 \text{ mM}$ against rat astrocytes and human glioblastoma, respectively.⁵² Further studies suggested that depletion of glutathione and induction of apoptosis were possible explanations for the cytotoxicity observed for catechol towards mouse neuroblastoma N2a cell line.⁵¹ These preliminary studies rationalize our choice to integrate catechol and its oxidation products into a Ru(II) polypyridyl complex. To the best of our knowledge, $[\text{Ru}(\text{DIP})_2(\text{sq})](\text{PF}_6)$ is the first Ru(II) polypyridyl complex containing a catechol moiety to be deeply investigated from both a physico-chemical and biological point of view. As described in this work, *in vitro* and *in vivo* studies demonstrate a significant potential of this compound as a chemotherapeutic agent against cancer.



Scheme 1. a) Synthesis of $[\text{Ru}(\text{DIP})_2(\text{sq})](\text{PF}_6)$. I) DIP, LiCl, DMF, reflux, 24 h, 78%; II) (i) NaOH, catechol 2-propanol, reflux, 24h; (ii) air, 2 h; (iii) NH_4PF_6 , 2-propanol/ H_2O (1:8), 19%. b) Catechol (cat) and its oxidised forms, semiquinonate (sq) and quinone (q).

Results and Discussion

Synthesis and characterization of [Ru(DIP)₂(sq)](PF₆)

The synthesis of the target compound [Ru(DIP)₂(sq)](PF₆) was achieved in a 2-step synthesis (Scheme 1a). Briefly, the known Ru(DMSO)₂Cl₂⁵⁸, DIP and LiCl were refluxed in DMF to afford Ru(DIP)₂Cl₂ in 72% yield after precipitation with acetone.⁵⁹ The compound was then refluxed in a nitrogen atmosphere overnight with catechol in the presence of NaOH in 2-propanol. The oxidation step of the catecholate to the semiquinonate was performed by exposing the solution of the Ru complex in 2-propanol to air for 2 h. [Ru(DIP)₂(sq)](PF₆) was obtained in 19% yield after precipitation with a large excess of NH₄PF₆ and purification *via* silica gel chromatography. The identity of the product was confirmed by HR-MS and NMR spectroscopy. ¹H-NMR spectra showed a characteristic peak broadening in the aromatic region between 7–9 ppm due to the paramagnetism of the complex. In the ¹³C NMR and 2D ¹H-¹³C HSQC spectra (Figure S1), ten inequivalent CH carbons were observed, suggesting an overall C₂ symmetry of the complex. The purity of the product was confirmed by microanalysis.

X-ray Crystallography of [Ru(DIP)₂(sq)](Cl)

The crystal structure of [Ru(DIP)₂(sq)](Cl) was determined by a single crystal X-ray diffraction study. Suitable single crystals were grown from slow diffusion of diethylether into a solution of the product prior to precipitation with NH₄PF₆ in MeCN. The crystal structure revealed two independent Ru molecules (Ru-1 and Ru-2 in Figure S2), two chloride counter ions (from LiCl) and three water molecules in the asymmetric unit (monoclinic *P*2₁/*c* space group). Both Cl atoms are disordered over two sets of

sites with site-occupancy ratios of 0.299/0.701(3) and 0.244/0.756(5). The H atoms of the isolated water molecules could be introduced in the final refinements, but their positions were kept fixed to satisfy reliable hydrogen bonding. The molecular structure of one of the independent Ru molecules is shown in Figure 1 and a selection of the most relevant bond lengths and angles are provided in Tables S1 and S2 (additional crystallographic information can be found in the supporting information). The X-ray crystal structure determination also provided evidence for the oxidation state of the dioxolene ligand, as it can exist in three different oxidation states; catechol, semiquinone and quinone.^{43,47,60} The typical range for the C-O bond length of such a ligand coordinated to a metal is 1.34–1.47 Å for the catechol form, 1.27–1.31 Å for the semiquinone form and around 1.23 Å for the quinone.^{43,60} The C-O bond distances of the dioxolene ligand in [Ru(DIP)₂(sq)](Cl) are 1.309(4), 1.314(4), 1.315(4) and 1.319(4) Å, which suggest that it is present in its semiquinone form.⁴³

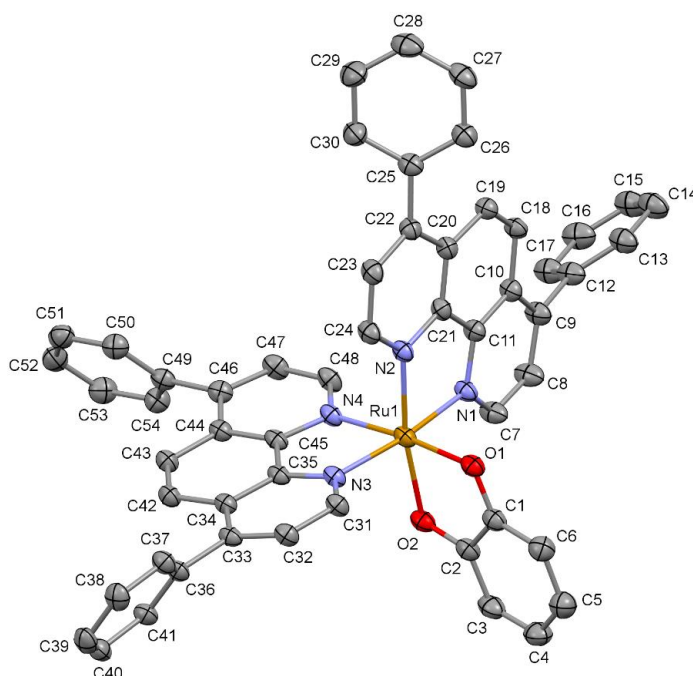


Figure 1. Molecular structure of [Ru(DIP)₂(sq)](Cl). The asymmetric unit contains two crystallographically independent Ru cations, only one of which is presented. The Cl⁻

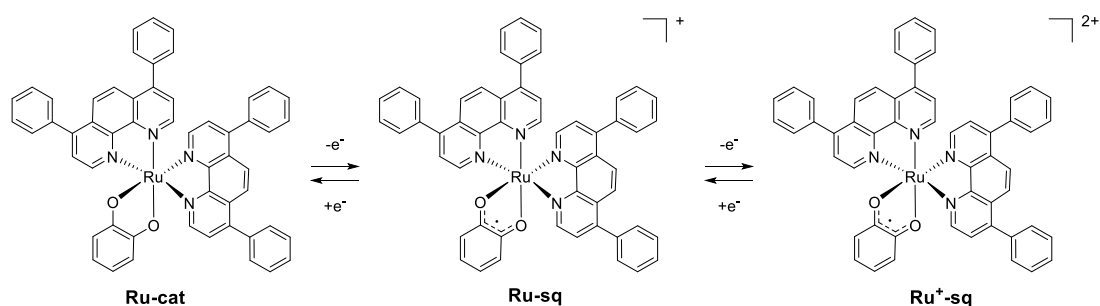
counter ions, H atoms and solvent molecules are omitted for clarity. The thermal ellipsoids are shown at the 30% probability level.

Electrochemistry

The electrochemistry of **[Ru(DIP)₂(sq)](PF₆)** (abbreviated as **Ru-sq**) was investigated using cyclic voltammetry (CV) and rotating disc electrode voltammetry (RDE) in DMF containing tetrabutylammonium hexafluorophosphate 0.1 M. The RDE voltammogram shown in Fig. S3 exhibits four well-defined, reversible waves, in addition to that of decamethylferrocene, which was used as internal reference with a half-wave potential of 0.030 V vs the Saturated Calomel Electrode (SCE). The four features related to the **Ru-sq** have the same intensity, which attests that the related redox processes involve the same number of exchanged electrons. By comparison with the data reported in the literature for closely related complexes under similar conditions,^{46,61,62} the underlying redox processes were assigned as shown in Table S3. The oxidation located at + 0.647 V vs SCE can be attributed to the Ru(II)/Ru(III) redox couple while the sq/cat redox couple can be associated to the first reduction process at -0.249 V vs SCE. The following two processes, at more negative potentials, can be assigned to the sequential reductions of the ancillary ligands (DIP^{0/-}). Of note, the latter are separate couples with quite some substantial redox splitting.^{46,61} These data clearly show how the presence of the semiquinonate ligand influences the redox properties of the metal centre, causing a shift to lower potential. The couple of Ru (III)-quinone ligand is not observed in these conditions since they are possibly located outside the anodic limit of a DMF-based electrolyte. Moreover, the CV experiment (Figure S3) indicates the reversibility of the redox processes, at least on the voltammetric timescale.

Electron Paramagnetic Resonance

Ru-sq in its native state is Electron Paramagnetic Resonance (EPR) active in DCM due to the presence of an unpaired spin as already confirmed by X-ray crystallography (Figure S4a). At room temperature, a rather broad isotropic signal was observed. Its g -value of 2.0244 is in line with a ligand-centred spin density and deviates only slightly from the free electron value g_e of 2.0023. This behaviour is in strong contrast to a metal-centred spin of a Ru(III) complex, which would only become observable at low temperatures due to rapid relaxation and display a broad, axial or rhombic signal with large anisotropy.^{47,63} The reduced form **Ru-cat** (Scheme 2) was generated by the reaction of **Ru-sq** with equimolar amounts of cobaltocene (Cp_2Co , $E_{1/2} = -0.880$ V vs SCE in DMF/0.1 M NBu_4PF_6) (Figure S4b).⁶⁴ Owing to the presence of a low-spin Ru(II) ion and a closed-shell catecholate ligand this species is EPR silent. The same holds also true for oxidized, dicationic **Ru⁺-sq** (Scheme 2), which was prepared by treatment of **Ru-sq** with an excess of 1,1'-diacetylferrocenium hexafluoroantimonate ($\text{Ac}_2\text{FcSbF}_6$, $E_{1/2} = 0.940$ V vs SCE in DMF/0.1 M NBu_4PF_6) (Figure S4c).^{64,65} The absence of an EPR signal indicates that the unpaired spins at the Ru(III) ion (**Ru⁺**) and the sq ligand are antiferromagnetically coupled.



Scheme 2. Structures of **Ru-cat**, **Ru-sq**, and **Ru⁺-sq**, carrying a catecholate or a semiquinonate ligand and Ru in oxidation state +II (**Ru**) or +III (**Ru⁺**), respectively.

Stability in DMSO and human plasma

The stability of a compound plays an important role in its biological activity and viability. Therefore, the integrity of **Ru-sq** was first assessed in DMSO-d⁶ using ¹H NMR spectroscopy. Spectra of **Ru-sq** were compared over 8 days, showing a complete stability of the complex (Figure S5). Next, to obtain a preliminary insight into the behaviour of **Ru-sq** under physiological conditions, the stability of **Ru-sq** in human plasma was investigated by UPLC following a procedure already established by our group.³⁷ **Ru-sq** was incubated in human plasma at 37°C for 0 h, 4 h, 6 h, 12 h, 20 h and 24 h using diazepam as an internal standard. The UV traces of the UPLC analysis are shown in Figure S6a. The concentration of **Ru-sq** was normalized with respect to the internal standard and plotted against time. The linear trend shown in Figure S6b clearly demonstrates that between 6 and 20 h, a decomposition of 50% of the compound was observed, to reach a total degradation of the compound after 24 h.

Cytotoxicity Studies

After a full characterisation of **Ru-sq**, its potential activity as a chemotherapeutic agent was investigated starting from the biological evaluation of its behaviour against cancer cells in monolayer cell cultures. The cytotoxicity of **Ru-sq** towards HeLa (human cervical) cell line, A2780 (human ovarian carcinoma), A2780 cis (human cisplatin resistant ovarian carcinoma), A2780 ADR (human doxorubicin resistant ovarian carcinoma), CT-26 (mouse colon adenocarcinoma), CT-26 LUC (mouse colon adenocarcinoma stably expressing luciferase), RPE-1 (human normal retina pigmented epithelial) and MRC-5 (human normal lung fibroblast) cell lines was therefore investigated using a fluorometric cell viability assay (single graphs available in Figures S7).⁶⁶ Cytotoxicity of cisplatin and doxorubicin was determined in the same cell lines as positive controls and, as additional controls, **Ru(DIP)₂Cl₂** and catechol were also

tested.^{67,68} As shown in Table 1 where IC₅₀ (the half maximal inhibitory concentration) values are reported, **Ru-sq** displayed IC₅₀ values in the nanomolar range for most of the cell lines investigated in this study, while the **Ru(DIP)₂Cl₂** precursor and the catechol ligand itself showed much lower cytotoxicity. Very impressively, **Ru-sq** exerted an activity 40 times higher than cisplatin against a cisplatin resistant cell line. On the other hand, the cytotoxicity of doxorubicin and **Ru-sq** against a doxorubicin resistant cell line appeared to be in the same order of magnitude. Overall, complex **Ru-sq** displays a cytotoxicity, which is comparable to doxorubicin and much higher than the one of cisplatin.

Table 1. IC₅₀ values of **Ru-sq**, the **Ru(DIP)₂Cl₂** precursor and the catechol ligand in tested cell lines; cisplatin and doxorubicin were used as positive controls.

IC ₅₀ (μM)	HeLa	A2780	A2780 ADR	A2780 cis	CT-26	CT-26 LUC	RPE-1	MRC-5
Cisplatin	9.28 ± 0.20	4.00 ± 0.76	8.32 ± 0.71	18.33 ± 2.92	2.60 ± 0.18	2.42 ± 0.23	30.24 ± 5.11	11.20 ± 2.32
Doxorubicin	0.34 ± 0.02	0.19 ± 0.03	5.94 ± 0.58	0.54 ± 0.04	0.082 ± 0.003	0.18 ± 0.006	0.89 ± 0.17	3.37 ± 1.24
Ru-sq	0.50 ± 0.01	0.67 ± 0.04	4.13 ± 0.2	0.45 ± 0.03	1.00 ± 0.03	1.51 ± 0.14	0.90 ± 0.04	0.95 ± 0.09
Ru(DIP)₂Cl₂	15.03 ± 0.4	4.69 ± 0.14	78.27 ± 4.9	6.36 ± 0.57	9.20 ± 1.22	6.65 ± 0.5	3.13 ± 0.07	5.54 ± 0.39
Catechol	>100	22.80 ± 5.96	>100	54.55 ± 11.30	16 ± 4.14	11.56 ± 0.40	>100	>100

Since **Ru-sq** exhibits promising activity in monolayer cell culture, we investigated its behaviour in a Multi Cellular Tumour Spheroids (MCTS) model.⁶⁹ It was previously shown that such a model mimics the *in vivo* microenvironment and tumour metabolism.^{70,71} Moreover, large MCTSs develop a central necrosis core similar to that found in the inner core of tumours.⁷² These unique features give a better representation

of a cancer model compared to a 2D model, lowering the disparity between *in vitro* and *in vivo* models.⁷² Table 2 shows the IC₅₀ values obtained *via* a luminescent cell viability assay for compounds that were administered to HeLa MCTSs for 48 h (single graphs are available in Figure S8). The **Ru(DIP)₂Cl₂** precursor and the catechol ligand were tested as additional controls and exhibited lower cytotoxicity than **Ru-sq**. Catechol resulted nontoxic with an IC₅₀ > 100 while the precursor displayed a cytotoxicity comparable to cisplatin. Cisplatin was used as a positive control and the results are in line with literature data.⁷³ The cytotoxicity of **Ru-sq** in HeLa MCTSs was impressively high after 48 h treatment, with IC₅₀ ~ 14 μM, which is 3 times lower than cisplatin or doxorubicin (IC₅₀ ~ 47 μM or 39 μM, respectively). Noteworthy, the cytotoxicity of **Ru-sq** was comparable to the one of doxorubicin after 72 h treatment (IC₅₀ ~ 11 μM).⁷⁴ These studies clearly demonstrate the high potential of **Ru-sq** as an anticancer drug candidate. The impressive bioactivity, comparable to doxorubicin in monolayer cell culture, was also confirmed in the 3D tumour model – HeLa MCTSs.

Table 2. IC₅₀ values for **Ru-sq**, **Ru(DIP)₂Cl₂** precursor and the catechol ligand in multicellular HeLa cancer cell spheroids (approximately 400 μm in diameter); cisplatin and doxorubicin were used as positive controls.

IC ₅₀ (μM)	Cisplatin	Doxorubicin	Ru-sq	Ru(DIP) ₂ Cl ₂	Catechol
HeLa MCTSs	46.49 ± 4.18	38.59 ± 0.43	14.11 ± 0.09	59.84 ± 3.05	>100

Spheroid integrity and growth upon treatment are very useful tools to determine a potential drug activity.⁷² In this study MCTSs were monitored over 13 days after treatment with different concentrations of **Ru-sq** (Figure 2). Every 3 days, the spheroids were washed to remove dead cells and their diameters were measured (Figure 2). It is important to note that at each washing step, half of the media was removed and

replaced with fresh one, diluting twice the quantity of the compound in each well. The effect of **Ru-sq** on growth inhibition is dose-dependent and already visible after 3 days. Low concentrations treatments (1 μM and 2.5 μM) led to regrowth of the spheroids after the first 72 h, while for 5 μM and 10 μM treatments, the regrowth is visible after 6 and 9 days, respectively. **Ru-sq** treatment with concentrations higher than IC_{50} (20 μM and 25 μM) completely inhibits the spheroids growth after 13 days of treatment. Overall, we can conclude that **Ru-sq** treatment at 20 μM and 25 μM concentrations, severely affect the size and the integrity of the spheroids after 13 days of treatment.

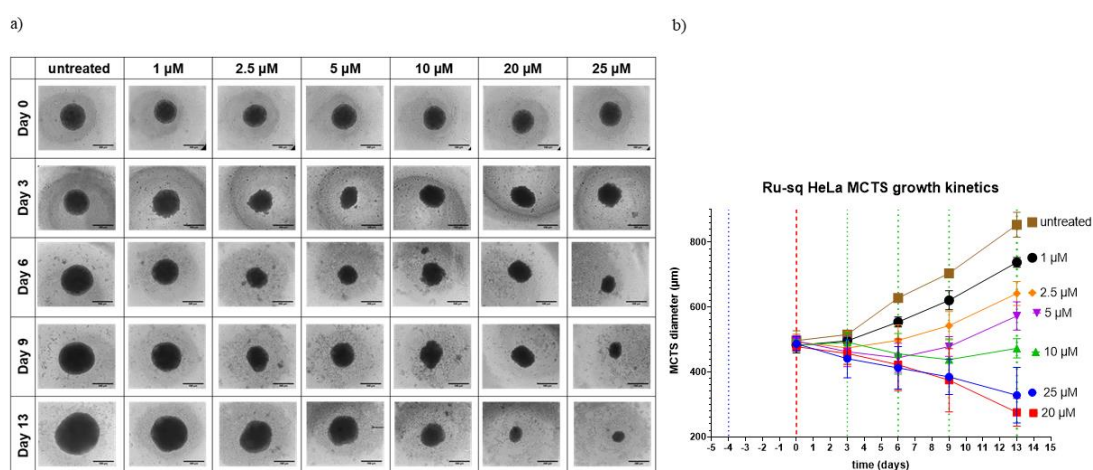


Figure 2. Growth kinetics of HeLa MCTSs upon treatment with different concentrations of **Ru-sq** (1, 2.5, 5, 10 and 20 μM). a) Images collected at day 0 (before treatment) and at day 3, 6, 9 and 13. b) MCTSs diameter calculated at different time points. Blue dotted line indicates day of seeding, red dashed line indicates day of treatment, green dotted lines indicate days of washing.

Cell Death Mechanism

The excellent activity displayed by **Ru-sq** in HeLa MCTSs encouraged us to perform further experiments in order to obtain more insights into its *in vitro* behaviour. The first step was the evaluation of the type of cell death occurring when cancer cells were

treated with **Ru-sq**. For this experiment, the Annexin V and PI staining method was used in HeLa cells.⁷⁵ Staurosporin, a known inducer of apoptosis, was employed as a positive control.⁷⁶ As shown in Figure 3 and Figure S9, **Ru-sq** induced significant apoptosis as early as 30 min treatment with progression from early to late apoptosis at 4 h. The level of apoptosis induction by the complex after 4 h was comparable to that caused by 24 h staurosporine treatment. These data clearly demonstrate that **Ru-sq** induces apoptosis as the only type of cell death in HeLa cells.

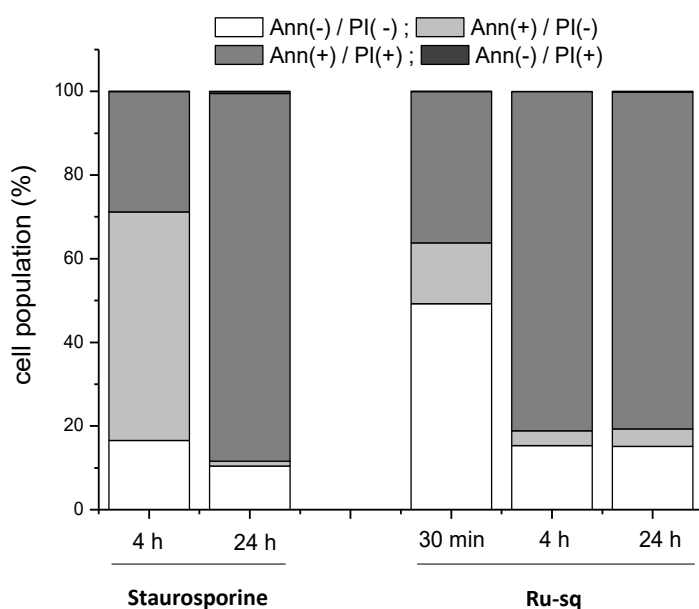


Figure 3. Induction of apoptosis/necrosis in HeLa cells upon treatment with **Ru-sq** (10 μ M) and staurosporine (1 μ M) at different time frames. The white area represents living cells (Annexin V, PI negative), the light grey displays early apoptotic cells (Annexin V positive, PI negative), the dark grey late apoptotic or dead cells (Annexin V and PI positive).

Cellular uptake

Next, the cellular uptake of **Ru-sq** was investigated in HeLa cells. The amount of ruthenium accumulated was detected by Inductively Coupled Plasma Mass

Spectrometry (ICP-MS). Working concentrations and incubation times were chosen to avoid extended cell mass loss due to the high cytotoxicity of the complexes but considering a ruthenium final amount that could afford determination of the metal content. Nearly 70 % of internalisation was found in HeLa cells after 2 h treatment (5 μ M) with **Ru-sq** (Figure 4a). On the other hand, only 48% of the ruthenium was taken up when cells were treated with the **Ru(DIP)₂Cl₂** precursor (Figure 4b). To have more insights into mechanisms that leads to the accumulation of **Ru-sq** into the HeLa cells, additional experiments were performed in the presence of different inhibitors of uptake pathways. Low temperature (4°C), blocked cellular metabolism (2-deoxy-*D*-glucose, oligomycin), impede endocytic pathways (chloroquine or ammonium chloride) or stopped cation transporters (tetraethylammonium chloride) abolished or significantly decreased **Ru-sq** accumulation in cells (see Figure S10). This outcome indicates that **Ru-sq** is actively transported into HeLa cells. Further cellular fractionation experiment showed preferential accumulation of **Ru-sq** inside the nucleus (74%) (Figure 4c), which suggests that the mode of action could be related to the damage caused to DNA and/or to prevention of replication as well as transcription.^{77,78} The second preferential site of accumulation for **Ru-sq** were mitochondria (17%) suggesting that the metabolism impairment might also contribute to the cell death.⁷⁹

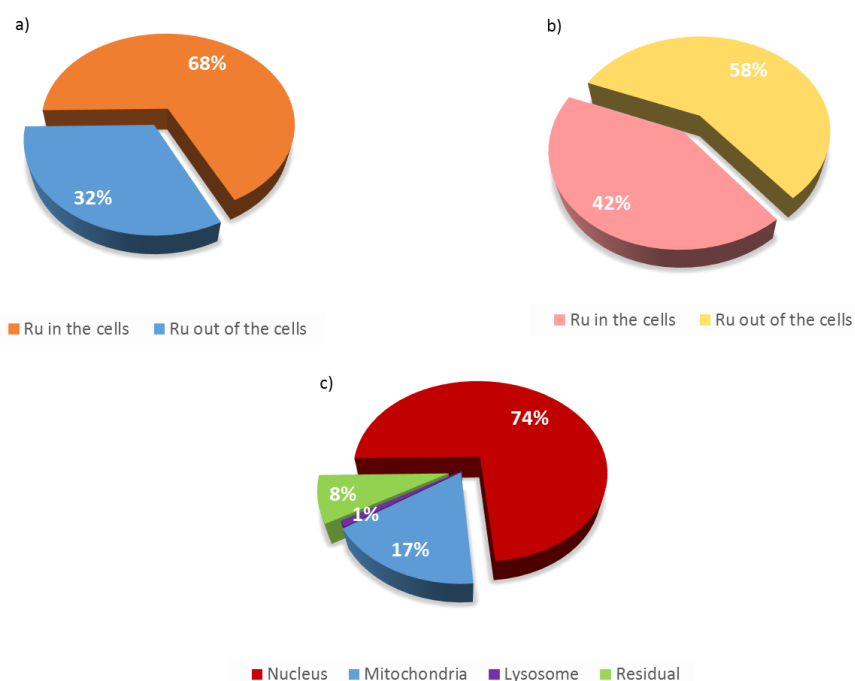


Figure 4. (a) Ruthenium cellular uptake in cells treated with **Ru-sq**, (b) Ruthenium cellular uptake in cells treated with the **Ru(DIP)₂Cl₂** precursor (c) Fractionated subcellular uptake of ruthenium in HeLa cells treated with **Ru-sq**. Results were obtained by incubating cells with 5 μ M of the target ruthenium complex for 2 h.

DNA Ruthenation

The preferential accumulation of **Ru-sq** in the nucleus led to further studies to identify DNA as a potential target for the complex. The genetic material was extracted from HeLa cells after 2 h treatment with **Ru-sq** and the **Ru(DIP)₂Cl₂** precursor. The amount of ruthenium in both DNA samples was determined by ICP-MS (Figure 5). The DNA of cells treated with the **Ru-sq** displayed a ruthenium content two times higher than in the cells treated with the **Ru(DIP)₂Cl₂** precursor.

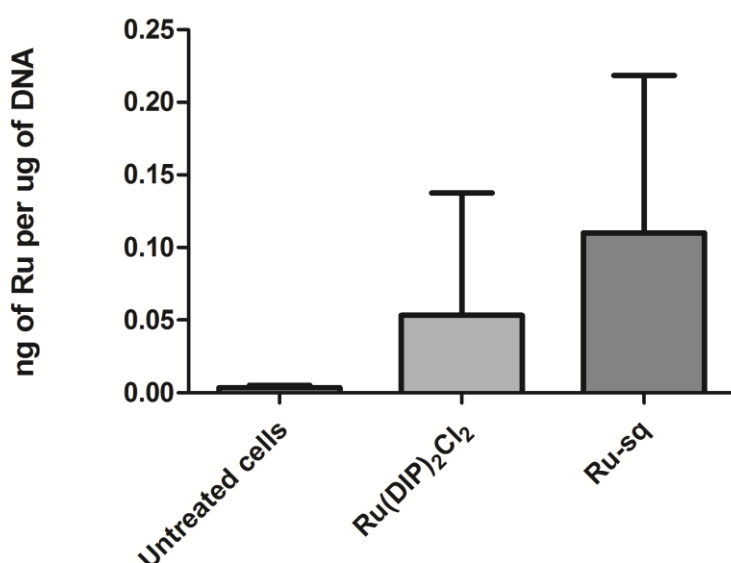


Figure 5. DNA ruthenation of the HeLa cells treated with **Ru-sq**, **Ru(DIP)₂Cl₂** precursor (2 h at 5 μ M concentration). Data is presented as the mean \pm SD of at least 3 independent experiments.

JC-1 Mitochondrial Membrane Potential Test

Due to the accumulation of **Ru-sq** in the mitochondria, further investigation on the impairment of the function of this organelle was undertaken. JC-1 is a membrane-permeant dye, which is largely used as an indicator of mitochondrial membrane potential.^{80,81} At high potentials, the dye forms red emitting aggregates in the mitochondria membrane, whereas at low potentials, it stays as a green emitting monomer.^{80,81} The membrane potential is directly connected to oxidative phosphorylation (the main mitochondrial function).⁸² HeLa cells were treated for 24 h with increasing concentrations of **Ru-sq** (from 0.2 μ M to 0.6 μ M). Figure 6 shows a slight decrease of the red fluorescence signal with increasing concentrations of **Ru-sq** and a significant drop in the signal around the IC₅₀ concentration (0.5 μ M, marked in

red). However, the dramatic collapse of mitochondrial membrane potential could also be caused by ongoing apoptosis.⁸³ Carbonyl cyanide 4-(trifluoromethoxy)phenylhydrazone (FCCP), an uncoupling agent that destroys the membrane potential⁸⁴ was used as positive control.⁸⁴ Comparison of the results obtained with **Ru-sq** (0.5 μ M) and FCCP treatment showed that the same loss in potential was detected. These findings strongly suggest a contribution of the membrane potential impairment to the cell death mechanism.

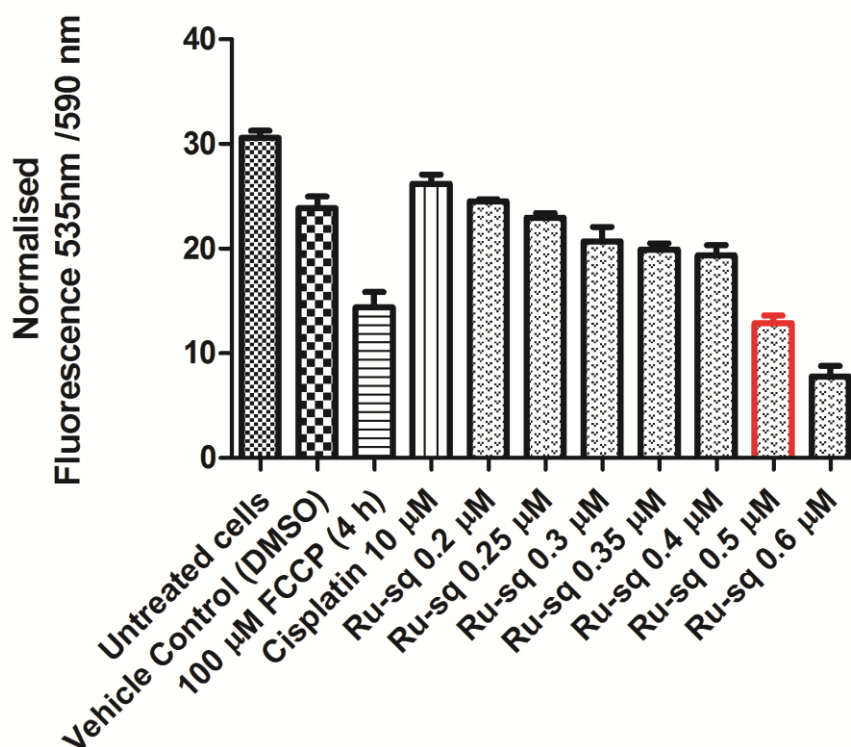


Figure 6. Fluorescence signal of JC-1 dye detected in HeLa cells treated for 24 h with different concentrations of **Ru-sq** (from 0.2 μ M to 0.6 μ M). Bar marked in red indicates the IC_{50} concentration (0.5 μ M). FCCP is used as positive control, cisplatin and DMSO (1%) are used as negative controls.

Mitochondrial Metabolic Studies

The accumulation of **Ru-sq** in mitochondria in HeLa cells (17%) and the impairment of the mitochondrial membrane potential prompted us to further study metabolic pathways that could be affected by the complex. For this purpose, Seahorse XF Analyzer was used to measure in real time oxygen consumption rate (OCR) and extracellular acidification rate (ECAR) in treated cells. Firstly, the effect of **Ru-sq** on the mitochondrial metabolism (oxidative phosphorylation) in the HeLa cell line was investigated. The effect on the other metabolic pathways, i.e. glycolysis and the possible metabolic modulation of the three primary fuel pathways, i.e. glucose, glutamine and fatty acid were then examined. Mitochondrial respiration was found to be severely impaired in cells treated with complex **Ru-sq** as opposed to the precursor **Ru(DIP)₂Cl₂**. This appeared evident from the low basal respiration, compared to untreated cells. ATP production was also inhibited by **Ru-sq**. The mitochondrial membrane lost the capacity to restore the proton balance when treated with an uncoupling agent (FCCP), the maximal respiration (the OCR value when the mitochondrial membrane is uncoupled) and spare respiratory capacity (difference of the OCR values between maximal respiration and basal respiration) of the cells was reduced compared to untreated cells (Figure 7 and Figure S11). All these effects point to disrupted mitochondrial respiration in cervical cancer cells caused by the complex. In contrast, the cell glycolysis, which is a cytosolic process, was not affected by **Ru-sq** (Figure S12). Additionally, due to very low oxygen consumption rate in cells treated with **Ru-sq**, direct effect on the 3-primary fuel pathways could not be determined (Figure S13). Hence, metabolic studies showed that the accumulation of **Ru-sq** in mitochondria has a significant role in the impairment of the oxidative phosphorylation. This effect, together with the results obtained by the JC-1 staining, strongly suggests

mitochondrial dysfunction as one of the modes of action of **Ru-sq**. In contrast, the chemotherapeutic drug cisplatin had no significant effect on the mitochondrial metabolism of HeLa cells. These observations points to the fundamental differences of mode of action of the **Ru-sq** and cisplatin that covalently binds to the nuclear DNA and inhibit the replication process. It is also widely known that DNA crosslinks can be repaired by different mechanisms like the nucleotide excision repair (NER) that eventually lead to drug resistance of the cancer cells. **Ru-sq**, with its multiple cellular targets, could potentially evade the repair pathways and circumvent such drawbacks associated with cisplatin.

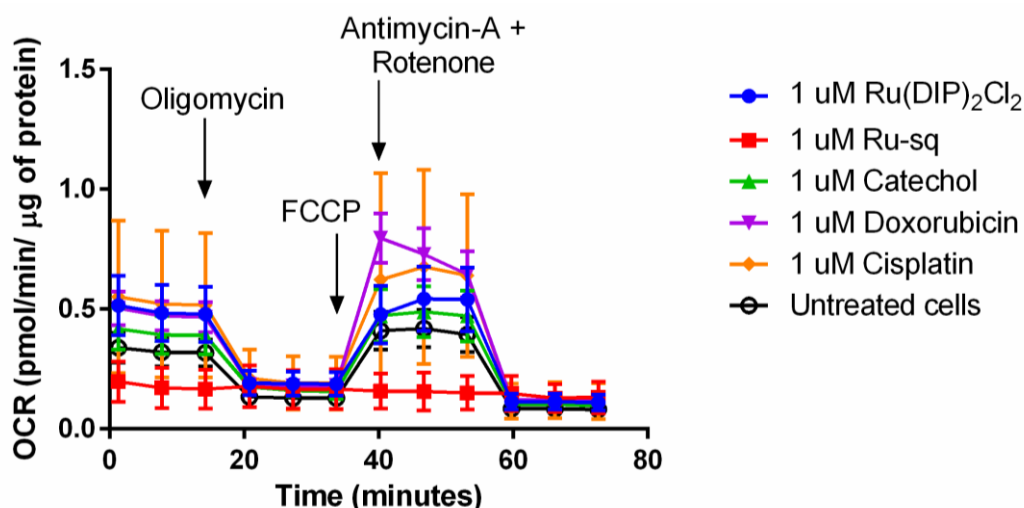


Figure 7. Mito Stress Test profile in HeLa cells after 24 h treatment; oxygen consumption rate changes after treatment with specific electron transport chain inhibitors. Oligomycin (inhibitor of ATP synthase (complex V)), FCCP (uncoupling agent), Antimycin-A (complex III inhibitor) and Rotenone (complex I inhibitor).

***In vivo* efficacy studies**

It is very difficult to evaluate selectivity of the anticancer drugs *in vitro*, as the proliferation of non-malignant cells is greatly affected by non-physiological conditions of cell culture in 2D and 3D models. The promising results obtained in studies conducted *in vitro* justified the assessment of **Ru-sq** efficacy in the context of whole organism. To this end, we performed *in vivo* studies to evaluate the effect on both tumour growth and survival of tumour-bearing mice. The doses were selected according to the dose-finding study, which had revealed a maximum tolerated dose (MTD) of 15 mg/kg of body weight. Two distinct models for testing *in vivo* efficacy of antitumor drugs are possible: a syngeneic (mice) tumour growing in a naturally immunocompetent mouse, or human tumour cells growing in immunodeficient animals. As both approaches have its advantages and pitfalls, we decided to use both models in this study.

Effect of Ru-sq on the growth of Ehrlich mammary carcinoma in immunocompetent NMRI mice and survival of tumour bearing mice

Even though the use of syngeneic tumour allografts in naturally immunocompetent animals had been often considered inferior during the era of athymic mice models, this method made a comeback as the necessity of diversified, near-physiological experimental sets was recognised. In this model, we can observe the effect of the tested compound within the context of the genuine immune system that plays a key role in tumour resistance.⁸⁵

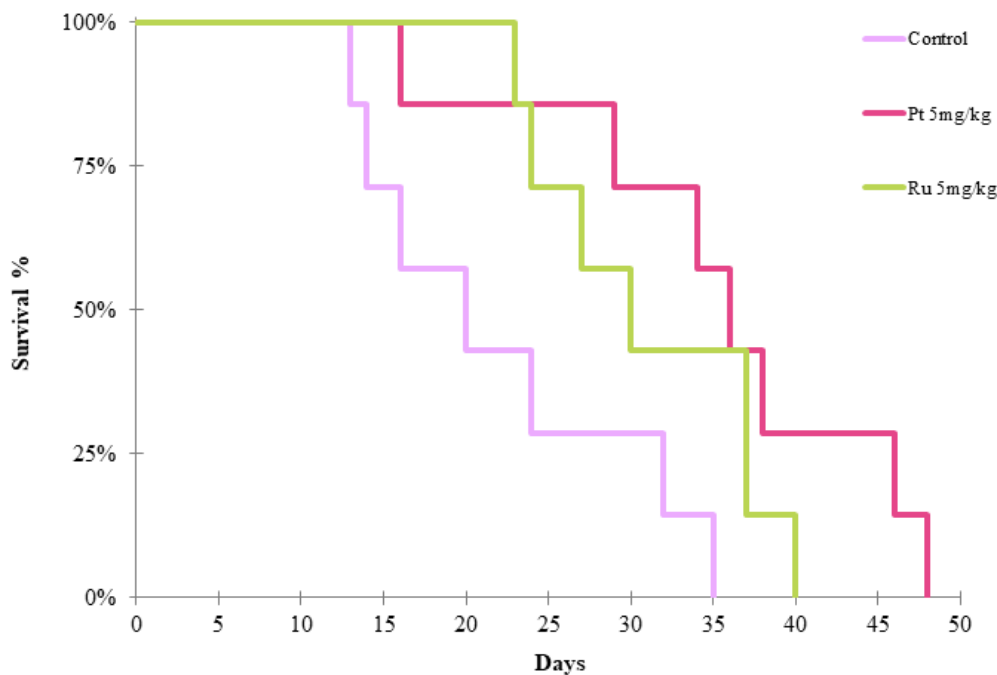


Figure 8. Kaplan-Meier analysis of survival of immunocompetent NMRI mice bearing Ehrlich carcinoma. Only the administration of complex **Ru-sq** 5 mg/kg i.p. and that of cisplatin (5 mg/kg) significantly prolonged the survival of tumour bearing mice when compared with the mixture of co-solvent and water. The compounds were administered i.p. on days 1 and 7 after tumour inoculation, n = 7 in each group.

During the study of the effect on the survival of immunocompetent NMRI mice bearing Ehrlich carcinoma (Figure 8), it was observed that the geometric mean of the overall survival of tumour bearing mice without therapy was 20.6 days. Among the three doses of **Ru-sq** tested, only 5 mg/kg prolonged the survival time significantly when compared with untreated tumour-bearing control mice (geom. mean = 31.9 days, $P = 0.033$). 10 mg and 15 mg/kg of **Ru-sq** seemed to exceed the optimal dose, causing a non-significant prolongation of survival ($P > 0.05$), with the geometric means of 30.2 and 25.5 days, respectively. The positive control cisplatin appeared to have similar efficacy (geom. mean = 33.7 days, $P 0.014$). An interesting and rare phenomenon was observed

in all three groups of **Ru-sq**. Although the tumour was advanced in the later stage of the experiment, all mice treated with **Ru-sq** showed active behaviour, little cachexia and unsuppressed food consumption.

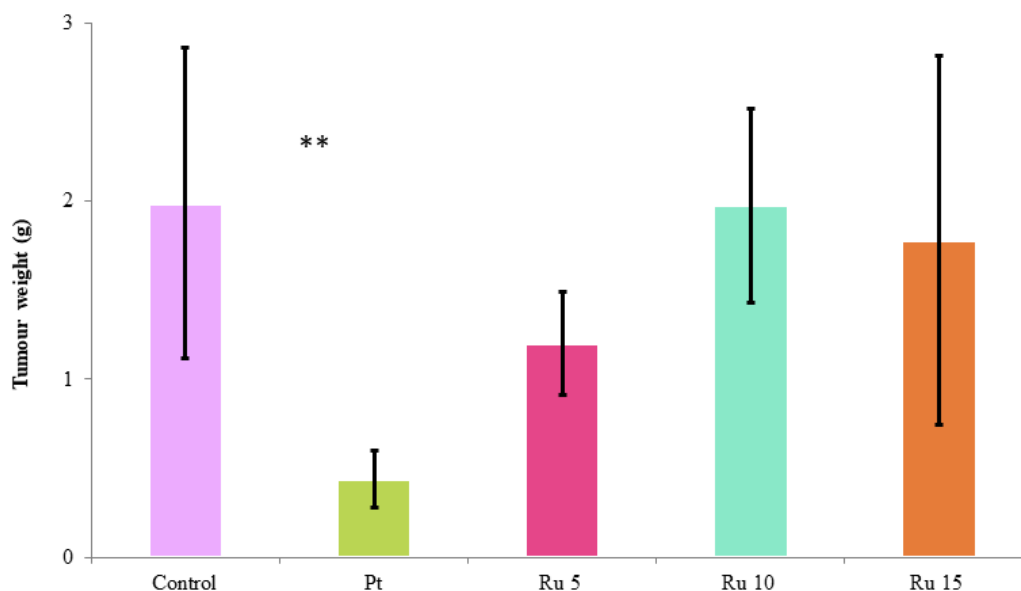


Figure 9. The weight of the solid Ehrlich tumour (in grams) on day 10 of mice injected on days 1 and 7 i.p. with pure vehicle, **Ru-sq** or cisplatin. Values are the means \pm SEM (n = 7 in each group). Control – tumour-bearing control treated with mixture of co-solvent and water; Pt – cisplatin 5 mg/kg i.p.; Ru 5 – **Ru-sq** 5 mg/kg i.p.; Ru 10 – **Ru-sq** 10 mg/kg i.p.; Ru 15 – **Ru-sq** 15 mg/kg i.p. Significantly different from the controls (**P < 0.01).

Furthermore, the effect of **Ru-sq** on tumour growth was examined. Figure 9 shows the weight of tumours at day 10 in mice treated with mixture of co-solvent and water, **Ru-sq** at 5, 10 or 15 mg/kg, or cisplatin at 5 mg/kg, and documents differences in the effect of the used drugs. Although only cisplatin exhibited a significant inhibitory effect on tumour growth ($P = 0.0011$), there was a slight but insignificant suppression at 5 mg/kg

Ru-sq ($P = 0.108$). As in the survival study, also here the optimum dose of **Ru-sq** seems to be in the lower part of the range tested.

Effect of Ru-sq on the growth of A2780 human ovarian cancer in immunodeficient nude mice and survival of tumour bearing mice

To compare the efficacy of the drug, therapeutic and survival experiment was repeated with athymic nude mice and human cancer line. A2780 human ovarian cancer cell line was chosen because of the use of cisplatin as comparative drug. Cisplatin is usually used for the therapy of ovarian cancer. Unfortunately, resistance often arises in treated patients. The use of human tumour xenografts in immunodeficient mice to examine therapeutic effect of potential chemotherapeutics, has several advantages. The major one is the use of actual human tumour tissue, featuring the complexity of genetic and epigenetic abnormalities that exist in the human tumour cell population.^{86,87} We evaluated the growth of A2780 human ovarian cancer cells in immunodeficient nude mice and their survival. Figure 10 shows the survival of animals; the longest average day of death is surprisingly associated to the negative control (42.88 ± 16.97 days). However, there was one surviving mouse in the group treated with **Ru-sq** 10 mg/kg and in the group treated with cisplatin. Two surviving mice were found in the group treated with higher dose of **Ru-sq** (15 mg/kg). Very interestingly, one of them was completely cured with no observable tumour.

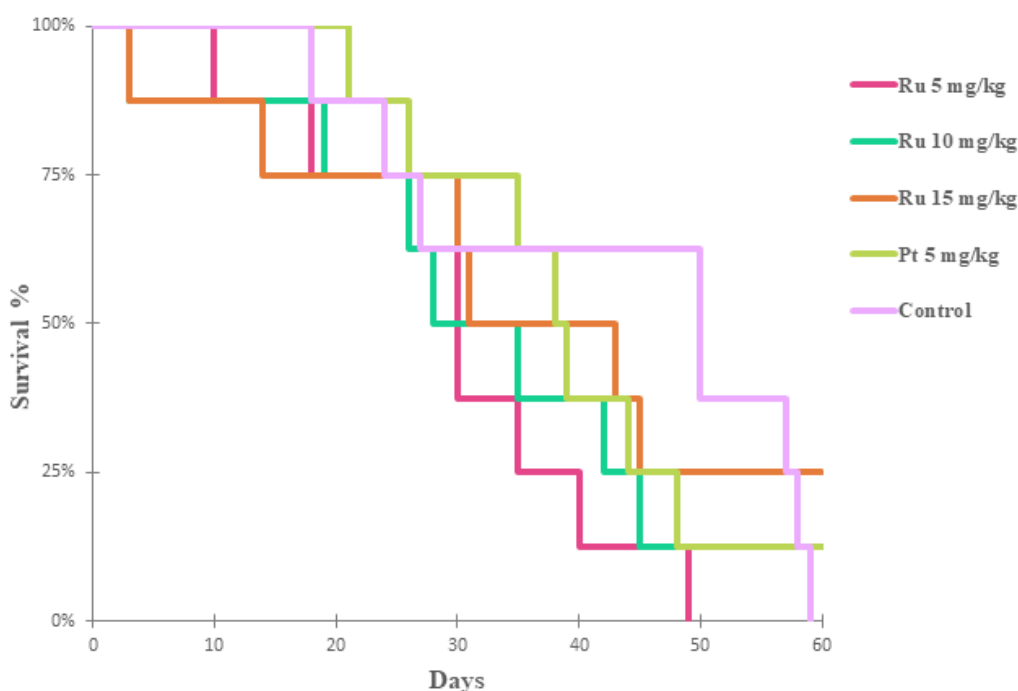


Figure 10. Tumour growth of A2780 cancer line in nude mice in first 15 days of therapy. Tumour size is shown as volume in cm^3 . Control – tumour-bearing control treated with mixture of co-solvent and water; Pt – cisplatin 5 mg/kg i.p.; Ru 5 – **Ru-sq** 5 mg/kg i.p.; Ru 10 – **Ru-sq** 10 mg/kg i.p.; Ru 15 – **Ru-sq** 15 mg/kg i.p. The most significant slowing down of tumour growth is observable in the group with **Ru-sq** 15 mg/kg.

Looking at the effect of **Ru-sq** on tumour growth (Figure 11), we observed that during the first days of therapy (day 4), there is a significant difference between groups treated with **Ru-sq** 15 mg/kg and cisplatin ($P = 0.00675$). Similar results between these two groups were observed at days 11 and 15 ($P = 0,04246$ for day 11 and $P = 0,0262$ for day 15). Comparison with untreated control group showed significant differences at days 11 and 15 ($P = 0.024$ for day 11; $P = 0.00931$ for day 15). **Ru-sq** administered in the dose of 15 mg/kg also showed decrease in tumour size over 15 days. Very interestingly, one mouse of this group was completely cured, no tumour volume was observed on the day 36 until the end of the experiment (day 60, data not shown).

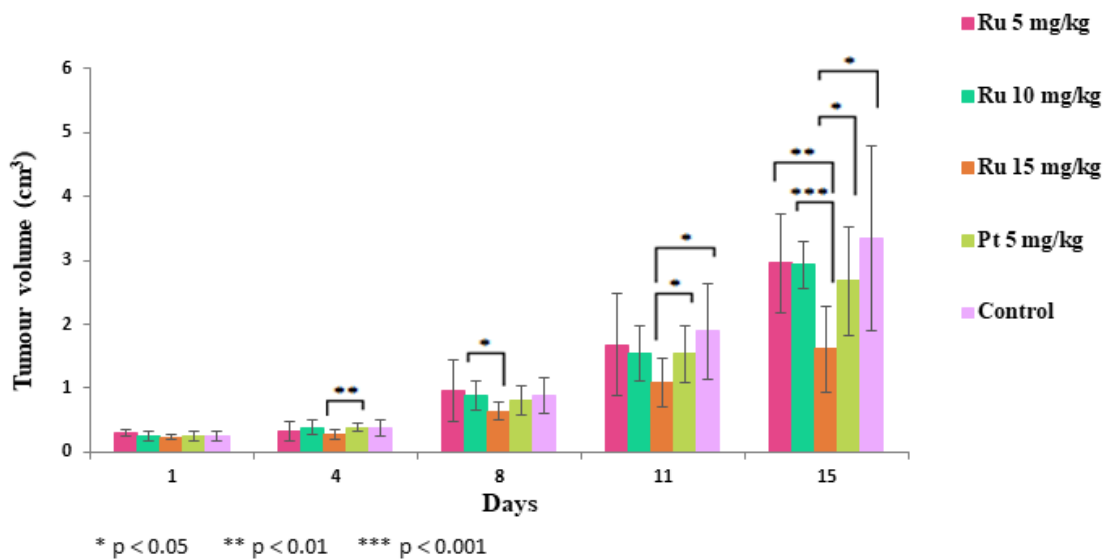


Figure 11. Tumour growth of A2780 cancer line in nude mice in first 15 days of therapy. Tumour size is shown as volume in cm^3 . Control – tumour-bearing control treated with mixture of co-solvent and water; Pt – cisplatin 5 mg/kg i.p.; Ru 5 – **Ru-sq** 5 mg/kg i.p.; Ru 10 – **Ru-sq** 10 mg/kg i.p.; Ru 15 – **Ru-sq** 15 mg/kg i.p. The most significant slowing down of tumour growth is observable in the group with **Ru-sq** 15 mg/kg.

These data demonstrate that the group treated with **Ru-sq** 15 mg/kg experienced a healing effect (in some points better than cisplatin), warranting further research. **Ru-sq** in a dose of 15 mg/kg has shown great potential to be an alternative and better drug candidate than cisplatin.

Taken together, we might conclude that in both models used **Ru-sq** reduces the growth of tumour cells and prolongs tumour-bearing mice survival, although the optimal dose would be different depending on strain of the mice and tumour type.

Akt-1 protein levels in HeLa cells

The interesting results obtained during the *in vivo* studies led us to further investigate the influence of **Ru-sq** on cell proliferation and/or migration. Akt is a serine/threonine kinase that promotes cellular survival.⁸⁸ Three isoforms of this protein exist in mammalian cells: Akt-1, Akt-2 and Akt-3.⁸⁹ Despite their high sequence similarity, they exhibit unique functions.⁹⁰ Akt-1 was found to be involved in the regulation of cell proliferation, transformation and tumour metastasis.⁹⁰ In this study, we assessed the influence of different concentrations (IC_{50} concentration and lower) of **Ru-sq** and **Ru(DIP)₂Cl₂** on Akt-1 protein levels in HeLa cells. The concentrations chosen for the treatment were rationalised in order to avoid false results triggered by the occurrence of cell death. As shown in Figure 12, the treatment with both complexes at all tested concentrations decreases the Akt-1 protein levels. Cisplatin and doxorubicin exhibited a much lower effect compared to our complexes at IC_{50} concentrations (IC_{50} = 10 μ M, IC_{50} = 0.3 μ M and IC_{50} = 0.5 μ M, respectively for cisplatin, doxorubicin and **Ru-sq**). These results fully support **Ru-sq** as promising chemotherapeutic agent. Further studies will be needed to fully understand the influence of our compound on cell proliferation and/or migration.

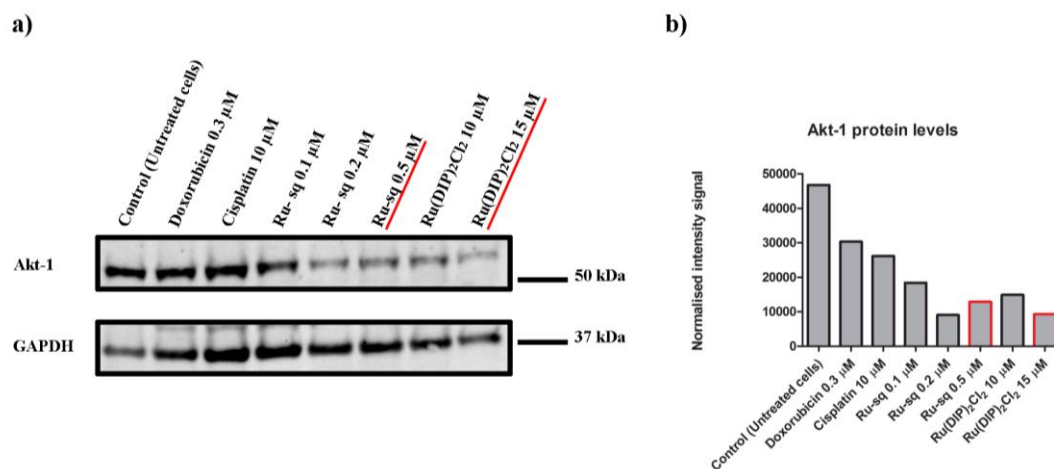


Figure 12. Western blot analysis of Akt-1 protein levels in HeLa cell line after 24 h treatment with different concentrations of **Ru-sq** and **Ru(DIP)₂Cl₂**. Cisplatin, doxorubicin and untreated cells were used as controls. The positions of the nearest molecular weight markers are indicated (a). Akt-1 protein levels normalised to GAPDH signal (b). The IC₅₀ concentrations of the two complexes are marked in red.

Conclusions

Ru-sq was successfully synthesised and fully characterised. Crystal structure, electrochemical and EPR studies confirmed the oxidation state of the dioxoligand (semiquinonate), which led to an overall positive charge of the complex. **Ru-sq** was found to be stable at room temperature in DMSO solution over one week and to have a half-life of 12 h upon incubation in human plasma at 37 °C. Cytotoxicity studies were performed in both, cellular monolayer (2D) and Multi Cellular Tumour Spheroids (MCTS) (3D) model. The cytotoxicity in 2D model was tested against different cell lines showing higher activity than cisplatin with IC₅₀ values mostly in the nanomolar range. The cytotoxicity in HeLa MCTSs confirmed the higher activity compared to cisplatin. Great tumour inhibition growth was observed after treatment with **Ru-sq** at concentrations 20 µM and 25 µM. Deeper investigation revealed apoptosis as main cause of cell death. **Ru-sq** was found to be taken up by HeLa cells more efficiently than **Ru(DIP)₂Cl₂** precursor and accumulate preferentially in nucleus and mitochondria. DNA ruthenation studies points that **Ru-sq** might damage the DNA and/or prevent replication as well as transcription processes. Mitochondrial function upon **Ru-sq** treatment was also studied using an indicator of the mitochondrial membrane potential (JC-1) and mitostress test (Seahorse technology). From these studies, a severe impairment of the mitochondrial potential was observed suggesting the contribution of mitochondrial dysfunction to the mode of action of **Ru-sq**. *In vivo* studies were performed using two different models: a syngeneic (mice) tumour growing in a naturally immunocompetent mouse, or human tumour cells growing in immunodeficient animals. **Ru-sq** reduces the growth of tumour cells and prolongs tumour-bearing mice survival. However, the optimal dose would be different depending on strain of the mice and tumour type.

Overall, **Ru-sq** displayed better activity than cisplatin in 2D and 3D cell cultures as well as for some conditions used *in vivo*. In conclusion, in this work, we could demonstrate the promising potential expressed by **Ru-sq** as chemotherapeutic agent against cancer. We strongly believe that further studies might lead our compound to advance towards pre-clinical trials.

Experimental Section

Materials.

All chemicals were either of reagent or analytical grade and used as purchased from commercial sources without additional purification. Ruthenium trichloride hydrate was provided by I²CNS, 4,7-Diphenyl-1,10-phenanthroline, Lithium chloride (anhydrous, 99%), and catechol by Alfa Aesar, tetrabutylammonium hexafluorophosphate by Sigma-Aldrich. All solvents were purchased of analytical, or HPLC grade. When necessary, solvents were degassed by purging with dry, oxygen-free nitrogen for at least 30 min before use.

Instrumentation and methods.

Amber glass or clear glassware wrapped in tin foil were used when protection from the light was necessary. Schlenk glassware and a vacuum line were employed when reactions sensitive to moisture/oxygen had to be performed under nitrogen atmosphere. Thin layer chromatography (TLC) was performed using silica gel 60 F-254 (Merck) plates with detection of spots being achieved by exposure to UV light. Column chromatography was done using Silica gel 60-200 μm (VWR). Eluent mixtures are expressed as volume to volume (v/v) ratios. ¹H and ¹³C NMR spectra were measured on Bruker Avance III HD 400 MHz or Bruker Avance Neo 500 MHz spectrometers using the signal of the deuterated solvent as an internal standard.⁹¹ The chemical shifts δ are reported in ppm (parts per million) relative to tetramethylsilane (TMS) or signals from the residual protons of deuterated solvents. Coupling constants *J* are given in Hertz (Hz). The abbreviation for the peaks multiplicity is br (broad). ESI-HRMS experiments were carried out using a LTQ-Orbitrap XL from Thermo Scientific (Thermo Fisher Scientific, Courtaboeuf, France) and operated in positive ionization mode, with a spray voltage at 3.6 kV. Sheath and auxiliary gas were set at a flow rate

of 5 and 0 arbitrary units (a.u.), respectively. Applied voltages were 40 and 100 V for the ion transfer capillary and the tube lens, respectively. The ion transfer capillary was held at 275°C. Detection was achieved in the Orbitrap with a resolution set to 100,000 (at m/z 400) and a m/z range between 200-2000 in profile mode. Spectrum was analysed using the acquisition software XCalibur 2.1 (Thermo Fisher Scientific, Courtaboeuf, France). The automatic gain control (AGC) allowed accumulation of up to 2.105 ions for FTMS scans, Maximum injection time was set to 300 ms and 1 μ scan was acquired. 5 μ L was injected using a Thermo Finnigan Surveyor HPLC system (Thermo Fisher Scientific, Courtaboeuf, France) with a continuous infusion of methanol at 100 μ L.min⁻¹. Elemental analysis was performed at Science Centre, London Metropolitan University using Thermo Fisher (Carlo Erba) Flash 2000 Elemental Analyser, configured for %CHN. IR spectra were recorded with SpectrumTwo FTIR Spectrometer (Perkin–Elmer) equipped with a Specac Golden Gate™ ATR (attenuated total reflection) accessory; applied as neat samples; $1/\lambda$ in cm⁻¹. Analytical HPLC measurement was performed using the following system: 2 x Agilent G1361 1260 Prep Pump system with Agilent G7115A 1260 DAD WR Detector equipped with an Agilent Pursuit XRs 5C18 (100Å, C18 5 μ m 250 x 4.6 mm) Column and an Agilent G1364B 1260-FC fraction collector. The solvents (HPLC grade) were millipore water (0.1% TFA, solvent A) and acetonitrile (0.1% TFA, solvent B). The HPLC gradient used is the following: 0-3 minutes: isocratic 90% A (5% B); 3- 25 minutes: linear gradient from 90% A (5% B) to 0% A (100% B); 25-30 minutes: isocratic 0% A (100% B), 30-35 minutes: linear gradient from 0% A (100% B) to 95% A (5% B). The flow rate was 1 mL/min. Detection was performed at 215nm, 250nm, 350nm, 450nm, 550nm and 650nm with a slit of 4nm. Stability in human plasma was performed on HPLC (Acquity Ultra Performance LC, Waters) that was connected to a

mass spectrometer (Bruker Esquire 6000) operated in ESI mode. The ACQUITY UPLC BEH C18 Gravity 1.7 μm (2.1 \times 50 mm) reverse phase column was used with a flow rate of 0.6 ml/min and UV-absorption was measured at 275 nm. The runs were performed with a linear gradient of A (acetonitrile (Sigma Aldrich HPLC-grade)) and B (distilled water containing 0.1% formic acid): t = 0–0.25 min, 95% A; t = 1.5 min, 100% A; t = 2.5 min, 100% A. Fractionation ICP-MS measurements were performed on an Agilent QQQ 8800 Triple quad ICP-MS spectrometer (Agilent Technologies) with a ASX200 autosampler (Agilent Technologies), equipped with standard nickel cones and a “micro-mist” quartz nebulizer fed with 0.3 ml/min analytic flow (as a 2% HNO_3 aqueous solution). Cellular Uptake, mechanism of uptake and ruthenation of the DNA was performed using a High-Resolution ICP-MS Element II from ThermoScientific located within the Environmental Biogeochemistry team of the Institut de Physique du Globe de Paris. This ICP-MS enables working in different resolution modes (LR=400, MR=4000 and HR=10000) for a better discrimination between elements of interest and interferences.⁹²

For the metabolic studies Seahorse XFe96 Analyser by Agilent Technologies was used.

Synthesis and characterization.

Ru(DMSO)₂Cl₂. Ru(DMSO)₂Cl₂ was synthesised following an adapted literature procedure.⁵⁸ Spectroscopic data (¹H NMR) was in agreement with literature.⁵⁸

Ru(DIP)₂Cl₂. The complex was synthesised following an adapted literature procedure.⁵⁹ A mixture of Ru(DMSO)₂Cl₂ (3.0 g, 6.19 mmol), 4,7-diphenyl-1,10-phenanthroline (4.11 g, 12.38 mmol) and LiCl (2.0 g, 47.18 mmol) dissolved in DMF (100 mL) was refluxed for 24 h. After cooling to *r.t.*, the solvent was reduced *in vacuo* to 8 mL and 350 mL of acetone were added. The mixture was then stored at -20 °C overnight before filtration with a Buchner funnel and washed with Acetone and Et₂O

to afford Ru(DIP)₂Cl₂ as a deep purple solid (3.76 g, 4.49 mmol, 72%). Spectroscopic data (¹H NMR) were in agreement with literature.⁵⁹

[Ru(DIP)₂(sq)](PF₆) (Ru-sq).

Ru(DIP)₂Cl₂ (0.739 g, 0.88 mmol) and aq. NaOH (0.5 mL, 1 M) were dissolved in 2-propanol (40 mL). The solution was degassed for 15 min and catechol (0.155 g, 1.41 mmol) was added. The mixture was heated to reflux for 24 h under N₂ atmosphere and protected from light. After cooling to *r.t.*, the mixture was stirred opened to air while still protected from light and the solvent was removed under vacuum. The residual solid was dissolved in 2-propanol (7 mL) and H₂O (56 mL) and NH₄PF₆ (0.700 g, 4.3 mmol) were added. The mixture was stored in the fridge (4 °C) overnight. The precipitate was filtered with a Buchner funnel and washed with H₂O (3 x 50 mL) and Et₂O (3 x 50 mL). The solid was collected with DCM and dried under vacuum to deliver a crude product as the PF₆ salt (0.70 g), which was chromatographed on silica (DCM/MeCN 20:1 *R_f* : 0.3). Evaporation of the solvent under vacuum provided [Ru(DIP)₂(sq)](PF₆) as a deep red solid. Further wash with Et₂O and Heptane were necessary in order to obtain clean product. The solid with the washing solvent (10 mL) was sonicated for 10 min and then centrifuged. This procedure was repeated three times for each solvent. Finally the red solid was collected with DCM and dried under vacuum to afford a clean product (0.17 g, 0.167 mmol, 19%). IR (Golden Gate, cm⁻¹): 3345w, 1710m, 1600w, 1520s, 1455s, 1335s, 1270s, 1125s, 820s, 760m. ¹H NMR (400 MHz, CD₂Cl₂): δ/ppm = 8.79–8.20 (br, 5H, *arom.*), 8.09–7.88 (br, 5H, *arom.*), 7.73–7.42 (br, 14H, *arom.*), 7.26–6.92 (br, 10H, *arom.*), 6.92 – 6.63 (br, 2H, *arom.*). ¹³C NMR (125 MHz, CD₂Cl₂): δ/ppm = 149.84, 144.68, 136.10, 133.56, 130.36, 129.89, 129.53, 128.41, 126.21, 125.36, 121.47, 116.35. For the quaternary carbons, only two were observed in the ¹³C NMR spectrum where five were expected. This could be explained

by peak overlap or the signal being too weak to be detected within the acquisition time of the experiment which is common for quaternary carbons. HRMS (ESI+): m/z 874.1887 $[M - PF_6]^+$. Elemental Analysis: calcd. for $C_{54}H_{36}F_6N_4O_2PRu = C$, 63.65; H, 3.56; N, 5.50. Found = C, 63.62; H, 3.52; N, 5.45. HPLC: $T_R = 31.304$ min.

X-ray Crystallography.

Single-crystal X-ray diffraction data were collected at 183(1) K on a Rigaku OD XtaLAB Synergy, Dualflex, Pilatus 200K diffractometer using a single wavelength X-ray source (Mo $K\alpha$ radiation: $\lambda = 0.71073$ Å)⁹³ from a micro-focus sealed X-ray tube and an Oxford liquid-nitrogen Cryostream cooler. The selected suitable single crystal was mounted using polybutene oil on a flexible loop fixed on a goniometer head and transferred to the diffractometer. Pre-experiment, data collection, data reduction and analytical absorption correction⁹⁴ were performed with the program suite *CrysAlisPro*.⁹⁵ Using *Olex2*,⁹⁶ the structure was solved with the *SHELXT*⁹⁷ small molecule structure solution program and refined with the *SHELXL* program package⁹⁸ (version 2018/3) by full-matrix least-squares minimization on F^2 . *PLATON*⁹⁹ was used to check the result of the X-ray analysis.

Electrochemical Measurements.

The electrochemical experiments were carried out with a conventional three-electrodes cell (solution volume of 15 mL) and a PC-controlled potentiostat/galvanostat (Princeton Applied Research Inc. model 263A). The working electrode was a vitreous carbon electrode from Orignalys (France) exposing a geometrical area of 0.071 cm² and mounted in Teflon[®]. The electrode was polished before each experiment with 3 and 0.3 μ m alumina pastes followed by extensive rinsing with ultra-pure Milli-Q water. Platinum wire was used as counter electrode and saturated calomel electrode, SCE, as reference electrode. Electrolytic solutions, DMF containing tetrabutylammonium

hexafluorophosphate 0.1M (TBAPF₆, Aldrich, +99 %) as supporting electrolyte, were routinely deoxygenated by argon bubbling. All the potential values are given versus the calomel saturated electrode SCE and recalculated versus Me₁₀Fc^{0/+} potential value.

EPR.

Electron paramagnetic resonance (EPR) experiments were performed on a MiniScope MS400 table-top X-band spectrometer from Magnettech. Simulation of the experimental EPR spectra was performed with the MATLAB EasySpin program.¹⁰⁰ All samples were dissolved in dry and N₂-saturated DCM at a concentration of ca. 1 mM. Oxidized forms were generated using 1,1'-diacetylferrocenium hexafluoroantimonate (Ac₂FcSbF₆, $E_{1/2} = 0.940$ V vs SCE in DMF/0.1 M NBu₄PF₆).^{64,65} Chemical reduction was achieved by using cobaltocene (Cp₂Co, $E_{1/2} = -0.880$ V vs SCE in DMF/0.1 M NBu₄PF₆).⁶⁴

Stability studies.

The stability in DMSO-d₆ at room temperature was assessed by ¹H NMR over 8 days. The stability of **Ru-sq** in human plasma at 37 °C was evaluated following a slightly modified procedure already reported by our group.³⁷ The human plasma was provided by the Blutspendezentrum, Zurich, Switzerland. Diazepam (internal standard) was obtained from SigmaAldrich. Stock solutions of the complexes (20 mM) and diazepam (3.2 mM) were prepared in DMSO. For a typical experiment, an aliquot of the respective stock solutions and DMSO were then added to the plasma solution (975 μL) to a total volume of 1000 μL and final concentrations of 40 μM for the complexes and diazepam. The resulting plasma solution was incubated for either: 0, 4, 6, 12, 20, 24 or 48 h at 37°C with continuous and gentle shaking (ca. 600 rpm). The reaction was stopped by addition of 2 mL of methanol, and the mixture was centrifuged for 45 min

at 650g at room temperature. The methanolic solution was evaporated and the residue was suspended in 500 μ L of 1:1 (v/v) acetonitrile/H₂O solution. The suspension was filtered and analyzed using UPLC–MS with a total injection volume of 2 μ L.

Cell culture.

HeLa and CT-26 cell lines were cultured in DMEM media (Gibco). CT-26 LUC cell line was cultured in DMEM media (Gibco) supplemented with 1.6 mg/mL of Genticin. RPE-1 cell line was cultured in DMEM/F-12 media (Gibco). MRC-5 cell line was cultured in DMEM/F-10 media (Gibco). A2780, A2780 cis, A2780 ADR cell lines were cultured in RPMI 1640 media (Gibco). The resistance of A2780 cis was maintained by cisplatin treatment (1 μ M) for one week every month. The cells were used in the assays after one week from the end of the treatment in order to avoid interfered results. The resistance of A2780 ADR was maintained by doxorubicin treatment (0.1 μ M) once a week. Cells were used in the assays after three days post doxorubicin treatment in order to avoid interfered results. All cell lines were complemented with 10% of fetal calf serum (Gibco) and 100 U/mL penicillin-streptomycin mixture (Gibco) and maintained in humidified atmosphere at 37°C and 5% of CO₂.

Cytotoxicity Assay using a 2D cellular model.

Cytotoxicity of the tested **Ru-sq** and **Ru(DIP)₂Cl₂** complexes was assessed by a fluorometric cell viability assay using Resazurin (ACROS Organics). Briefly, cells were seeded in triplicates in 96-well plates at a density of 4×10^3 cells/well in 100 μ L. After 24 h, cells were treated with increasing concentrations of the ruthenium complexes. Dilutions for **Ru-sq** were prepared as follows: 2.0 mM stock in DMSO was diluted to 25 μ M with media and then filtrated (0.22 μ m filter VWR). For **Ru(DIP)₂Cl₂**

2.5 mM stock in DMF was prepared, which was further diluted to 100 μ M and filtrated (0.22 μ m filter VWR). After 48 h incubation, medium was removed, and 100 μ L of complete medium containing resazurin (0.2 mg/mL final concentration) was added. After 4 h of incubation at 37 $^{\circ}$ C, the fluorescence signal of resorufin product was read (ex: 540 nm em: 590 nm) in a SpectraMax M5 microplate Reader. IC₅₀ values were then calculated using GraphPad Prism software.

Generation of 3D HeLa MCTSs.

MCTS were cultured using ultra-low attachment 96 wells plates from Corning[®] (Fisher Scientific 15329740). HeLa cells were seeded at a density of 5000 cells per well in 200 μ L. The single cells would generate MCTSs approximately 400 μ m in diameter at day 4 with 37 $^{\circ}$ C and 5 % CO₂.

Treatment of 3D HeLa MCTSs.

HeLa MCTSs after 4 days of growing at 37 $^{\circ}$ C and 5 % CO₂ were treated by replacing half of the medium in the well with increasing concentration of compounds for 48 h in the dark. For untreated reference MCTS, half of the medium was replaced by fresh medium only. The cytotoxicity was measured by ATP concentration with CellTiter-Glo[®] Cell viability kit (Promega, USA).

CellTiter Glo[®] viability Test.

Cell viability for MCTSs was performed *via* ATP assay using luciferase. CellTiter-Glo[®] kit from Promega was used. The spheroids were incubated for 1 h after replacing half of the media with CellTiter-Glo reagent and the luminescence of the plate was read

by SpectraMax M5 microplate reader. IC₅₀ values were calculated using GraphPad Prism software.

HeLa MCTSs growth inhibition.

MCTSs were grown and treated as previously described (see above). MCTSs sizes were observed under a light microscope and pictures were taken with a Samsung Galaxy A5 2017 SM-A520FZKAXEF thanks to a phone microscope adaptor. Before imaging, the plate was shaken and half of the media was exchanged to remove dead cells. Images were recorded before treatment (day 0) and at day 3, 6, 9 and 13 after treatment. Pictures were first processed using GIMP a cross-platform image editor with a batch automation plug-in. The MCTSs sizes were then calculated with SpheroidSizer, a MATLAB-based and open-source software application to measure the size of tumour spheroids automatically and accurately. Data analysis was done using GraphPad Prism software.

Annexin V / PI assay.

The apoptosis and necrosis induction in HeLa cells treated with **Ru-sq** was evaluated *via* an AnnexinV/PI staining assay using flow cytometry and according to the manufacturer instructions with just minor changes (Sigma Aldrich, Cat. N°: APOAF). Briefly, the cells were seeded in a 100x15 mm Petri dish at density of 2×10^5 cells and cultured at 37°C / 6% CO₂ for 24 h. The medium was then removed and replaced with fresh medium containing 10 µM solution of medium containing complex **Ru-sq** and further incubated for 30 min, 4 h or 24 h. The cells were then trypsinised and pelleted, washed twice with ice cold PBS, centrifuged at 600g for 5 minutes, resuspended in 500 µL binding buffer (provided with the kit) and transferred FACS culture tube. 7.5 µL of Annexin V FITC complex solution (provided with the kit) and 10 µL of propidium

iodide (PI) solution (provided with the kit) were added. The samples were incubated for 15 minutes at room temperature (25°C) in the dark, 1000 µL of binding buffer were added and the probes analysed with a CynAn ADP9 flow cytometer with the FITC (for Annexin V-FITC, excitation = 488 nm, emission = 515-545 nm) and PE-Texas Red channels (for PI, excitation = 488 nm, emission = 564-606 nm) and. The data were analysed with Summit v4.3 software. Positive controls of cells treated with 1.0 µM of staurosporine for 4 h or 24 h recovery, respectively were performed.

Sample Preparation for cellular uptake.

HeLa cells were seeded at the density of 2×10^6 cells 24h prior to treatment. Next day cells were incubated with the compounds (5 µM for 2h). After that time cells were collected, washed with PBS and cell number was counted. Cells were spun down and cell pellet was snap freeze in liquid nitrogen. Samples were kept at -20 °C.

Sample Preparation for cellular fractionation.

HeLa cells were seeded a week before treatment at a concentration of 1×10^6 cells/ml in 15 cm² cell culture Petri dish, let grow until 80% of confluence and incubated with the target complex (previously dissolved in ethanol as vehicle, v/v < 0.1%) at a concentration of 5.0 µM for 2 hours. All the treatments were set up at the same concentration for comparative purposes. The medium was then removed, the cells washed with PBS and trypsinised. After re-suspension in PBS, the pellet was washed with ice cold PBS and collected per centrifugation (5910R, Eppendorf) at 500 g for 5 min at 4 °C. The organelles were then isolated via differential centrifugation. To separate lysosomes, a Lysosome Isolation Kit (Cat. Nr: LYSIS01, Sigma Aldrich) as well as the manufacturer procedure with minor modification was used. Briefly, the

collected pellets were redissolved in 2.0 ml of extraction buffer added with proteases cocktail (delivered with the kit) and incubated for 15 min on ice. The samples were then homogenized with a pre-chilled dounce homogenizer (7 ml, tight pestle A, 22 strokes) and centrifuged at 1000 g for 10 min at 4 °C.

After homogenization, the pellet obtained was redissolved in 2 ml of a sucrose solution (0.25 M sucrose, 10 mM MgCl₂) and layered with 2 ml of a second hypertonic sucrose solution (0.55 M sucrose, 0.5 mM MgCl₂). The suspension was centrifuged at 1450 g and 4 °C for 5 min. The pellet was re-suspended in 3 ml of the second sucrose solution and centrifuged at 1450 g and 4 °C for 5 min to obtain the nuclear extract. These steps of the isolation procedure were monitored under phase contrast microscope on Menzel-Gläser coverslips (Olympus IX81 microscope).

The supernatant was transferred in a fresh tube and centrifuged at 14000 g for 30 min at 4 °C. The pellet collected, dissolved in 1 mL of a 19% Optiprep Density Gradient Medium (present in the kit), added with a 250 mM solution of CaCl₂ (final concentration 8 mM) and centrifuged at 5000 g for 15 minutes at 4 °C to give the isolated lysosomal suspension. The intact lysosomal content was proofed with Neutral-Red Reagent (delivered in the kit) with dual-wavelength absorbance mode at 460 and 510 nm over a kinetic of 3 minutes in a Spectramax M5 microplate reader (Molecular Devices).

Mitochondria fractions were isolated via further differential centrifugation from the pellet non-containing lysosomes using a mitochondria extraction buffer (Cat. Nr.: E2778, Sigma Aldrich) following the manufacturer instructions. The samples were re-dissolved in 1.5 mL of extraction buffer and centrifuged at 11000 g for 10 minutes at 4 °C to obtained final pellets represented pure mitochondrial fractions.

All the fractions (mitochondria, lysosomes and nucleus) were isolated from the same

cellular sample for direct comparative purposes. The supernatant phases discarded during the isolation of nuclei, lysosomes and mitochondria procedures were collected and formed the “residual” fraction. An aliquot of crude lysate after homogenization, nuclear, mitochondrial (pellet lysed via freeze and thaw cycles followed by 20 minutes incubation in ultrasonic bath), lysosomal and residual fraction was each used for protein quantification using the Bradford method. The isolated samples were then lyophilized on an Alpha 2-4 LD plus (CHRIST). The resulting samples underwent chemical digestion with 10 mL of a 2% nitrohydrochloric acid solution for 24 h. The resulting suspensions were filtered on 0.20 µm non-pyrogenic sterile Filtropur filters (Sarstedt) and the obtained samples were injected in ICP-MS.

Cellular fractionation ICP-MS Studies.

Ruthenium was measured against a Platinum single element standard (Merck 1703410100) and verified by a control (Agilent5188-6524 PA Tuning 2). Ruthenium content of the samples was determined by means of a 7-step serial dilution in the range between 0 and 300 ppb in Ru ($R > 0.99$) with a background equivalent concentration of BEC: 6.3 ppt and a detection limit of DL: 17 ppt. Spiking the samples with untreated negative controls (to account for eventual carbon content from the biological samples) resulted in equivalent values within error ranges. A solution of Indium (500 ppb) and Tungsten (500 ppb) was used as internal standard. The results are expressed as ng Pt / mg protein (correction due to the different mass of the observed cellular compartments), as mean \pm standard deviation error of different independent experiments.

Sample preparation for mechanism of uptake studies.

Samples were prepared as previously reported.¹⁰¹ Briefly, HeLa cells were seeded at density of 2×10^6 and next day were pre-treated with corresponding inhibitors or kept at specific temperature for 1 h. After that time cells were washed with PBS and were incubated with $5 \mu\text{M}$ **Ru-sq** for 2 h (low temperature sample was kept at $4 \text{ }^\circ\text{C}$). Afterwards cells were washed with PBS, collected, counted and snap frozen in liquid nitrogen. Pellet was stored at $-20 \text{ }^\circ\text{C}$.

DNA ruthenation of HeLa cells.

Cells were seeded at density of 2×10^6 cells per 15 cm dish. The next day, cells were treated with the **Ru-sq** ($5 \mu\text{M}$) or **Ru(DIP)₂Cl₂** ($5 \mu\text{M}$) for 2 h. After that time, the cells were collected, snap frozen in liquid nitrogen and stored at $-20 \text{ }^\circ\text{C}$. The following day, DNA was extracted using a PureLink™ Genomic DNA Mini Kit (Invitrogen). The DNA purity was checked by absorbance measurements at 260 and 280 nm. Concentrations of genomic DNA was calculated assuming that one absorbance unit equals $50 \mu\text{g/mL}$. ICP-MS samples were prepared as follows: samples were digested using 70% nitric acid ($60 \text{ }^\circ\text{C}$, overnight) in 1:1.6 DNA to acid volume ratio. Samples were then further diluted 1:100 (1% HCl solution in MQ water) and analysed using ICP-MS.

ICP-MS studies of Cellular uptake, mechanism of uptake and DNA ruthenation.

Daily, prior to the analytical sequence, the instrument (sector-field inductively coupled plasma mass spectrometer, HR-ICP-MS Element II, ThermoScientific) was first tuned to produce maximum sensitivity and stability while also maintaining low Uranium oxide formation ($\text{UO}/\text{U} \leq 5\%$). Ruthenium stock solution (SCP Science, 1g/L) was diluted several times in 1% distilled hydrochloridric acid to obtain standards for the

calibration range (from 10 ng/L to 10 µg/L). Then, data were treated as follow: intensities were converted into concentrations using uFREASI (user-FRIENDly Elemental dAta proceSsIng).¹⁰² This software, made for HR-ICP-MS users community, is free and available on <http://www.ipgp.fr/~tharaud/uFREASI>.

JC-1 Mitochondrial Membrane Potential Test.

HeLa cells were seeded at a density of 6000 cells/ well in black 96 well-plate (costar 3916). The next day, the cells were treated with different concentrations of **Ru-sq** and **Ru(DIP)₂Cl₂**. After further 24 h, the cells were treated according to the JC-1 Mitochondrial Membrane Potential Assay Kit (Abcam, ab113850). The data were analysed using GraphPad Prism software.

Mito Stress Test.

HeLa cells were seeded in Seahorse XFe96 well plates at a density of 30,000 cells/ well in 80 µL. After 24 h, the media was replaced with fresh media and cisplatin (10 µM), catechol (10 µM), DIP (1 µM), complex **Ru(DIP)₂Cl₂** (10 µM) or complex **Ru-sq** (1 µM) were added. After 24 h of incubation, the regular media was removed and the cells were washed thrice using bicarbonate and serum free DMEM, supplemented with glucose, 1.8 mg/ mL; 1% glutamine and 1% sodium pyruvate and incubated in a non-CO₂ incubator at 37 °C for 1 h. Mito Stress assay was run using Oligomycin, 1 µM, FCCP 1 µM and mixture of Antimycin-A/ Rotenone 1 µM each in ports A, B and C respectively using Seahorse XFe96 Extracellular Flux Analyzer.

Glycolysis Stress Test.

HeLa cells were seeded in Seahorse XFe96 well plates at a density of 30,000 cells/ well in 80 μ L. After 24 h, the media was replaced with fresh media and cisplatin (10 μ M), catechol (10 μ M), DIP (1 μ M), complex **Ru(DIP)₂Cl₂** (10 μ M) or complex **Ru-sq** (1 μ M) were added. After 24 h of incubation, the regular media was removed and the cells were washed thrice using bicarbonate, glucose and serum free DMEM, supplemented 1% glutamine and 1% sodium pyruvate and incubated in a non-CO₂ incubator at 37 °C for an hour. Glycolytic stress test was run using glucose, 10 mM, Oligomycin, 1 μ M and 2-Deoxyglucose, 50 mM in ports A, B and C respectively using Seahorse XFe96 Extracellular Flux Analyzer.

Mito Fuel Flex Test.

HeLa cells were seeded in Seahorse XFe96 well plates at a density of 30,000 cells/ well in 80 μ L. After 24 h, the media was replaced with fresh media and cisplatin (10 μ M), catechol (10 μ M), DIP (1 μ M), complex **Ru(DIP)₂Cl₂** (10 μ M) or complex **Ru-sq** (1 μ M) were added. After 24 h of incubation, the regular media was removed and the cells were washed thrice using bicarbonate, and serum free DMEM, supplemented with 1.8 mg/mL glucose, 1% glutamine and 1% sodium pyruvate and incubated in a non-CO₂ incubator at 37 °C for an hour. Fuel flex assay for the different fuel pathways viz. glucose, glutamine and fatty acid was studied by measuring the basal oxygen consumption rates and that after addition of the inhibitor of the target pathway in port A and a mixture of the inhibitors of the other two pathways in port B. This gave a measure of the dependency of the cells on a fuel pathway. To study the capacity of a certain fuel pathway, the sequence of addition of the inhibitors was reversed. In port A was added the mixture of inhibitors for the other pathways and in port B was added the inhibitor for the target pathway. UK-5099 (pyruvate dehydrogenase inhibitor, 20 μ M) was used as an inhibitor for the glucose pathway. BPTES (selective inhibitor of

Glutaminase GLS1, 30 μ M) was used as an inhibitor for the glutamine pathway. Etomoxir (O-carnitine palmitoyltransferase-1 (CPT-1) inhibitor, 40 μ M) was used as an inhibitor for the fatty acid pathway.

Animals and Tumour Model for Ehrlich mammary carcinoma in immunocompetent NMRI mice.

Due to the poor solubility of Ru-sq in water, dimethyl sulfoxide (DMSO), 1.81 mL / kg of body weight, had to be added to water for injections, for which reason the i.p. route of administration was chosen rather than i.v. Female outbred mice (NMRI) were used for this study, they were obtained from Masaryk University (Brno, Czech Republic). Animal care was conformed to EU recommendations and in accordance with the European convention for the protection of vertebrate animals used for experimental and other scientific purposes; it was approved by the Ethical Commission of the Medical Faculty in Hradec Králové (Nr. MSMT-56249/2012-310). For the MTD assessment, two or three healthy mice per group were observed for weight loss (the limit was 10%) over 14 days after injection of the solution. For the in vivo activity study, 70 NMRI female mice, 7 weeks old and weighting in the average 31.8 g (SD = 1.27) were fed a standard diet and water ad libitum. A solid Ehrlich tumour was purchased from the Research Institute for Pharmacy and Biochemistry (VUFB) in Prague, and then maintained in NMRI mice by periodical transplantations. The homogenised tumour tissue was inoculated subcutaneously into all mice on day 0, using 0.2 mL of 1/1 (v/v) homogenate freshly prepared in isotonic glucose solution. The tumour-bearing mice were then divided into 5 groups of 14 animals as follows: a control group treated with the pure solvent (DMSO and water), 3 groups of animals treated with Ru-sq in doses of 5, 10, and 15 mg/kg i.p. and a positive controls receiving 5 mg/kg cisplatin i.p. (Cisplatin 50 ml/25 mg, EBEWE Pharma, Austria). The solutions were administered

on days 1 and 7 in volumes of 0.2 mL per 20 g body weight. On the tenth day, half of the mice were sacrificed, and their tumours were weighed. The remaining animals were left in order to observe their survival.

Statistical Analysis for Ehrlich mammary carcinoma in immunocompetent NMRI mice.

One-Way Analysis of Variance with post-hoc Dunnett's multiple comparison test was used to detect differences in tumour weight. Kaplan-Meier curves and logrank tests were used to compare survival times in groups. Here, the level of significance was $\alpha=0.05$. MS Excel 2003 and NCSS software was used for the calculations and statistical evaluations.

Animals and Tumour Model for A2780 human ovarian cancer in immunodeficient nude mice.

The animal experiment depicted here after were performed in accordance with the Act on Experimental Work with Animals (Public Notice of the Ministry of Agriculture of the Czech Republic No. 246/1992, No. 311/1997, No. 207/2004; Decree of the Ministry of the Environment of the Czech Republic No. 117/1987; and Act of the Czech National Assembly No. 149/2004), which is fully compatible with the corresponding European Union directives. Athymic nude mice were used for experiment (obtained from AnLab Ltd., Prague, Czech Republic, females, 8 weeks old, $n = 40$). After acclimatization, the A2780 human ovarian cancer cell line was implanted subcutaneously in the shaved right flank of mice (obtained from Sigma-Aldrich, Missouri, USA, used medium RPMI with 10 % fetal bovine serum, 2×10^6 cells per mouse applicated with cells to Matrigel ratio 2:1). The animals were randomly divided into five groups ($n = 8$), when tumour

reached the size of 5 – 8 mm in diameter. 5 % DMSO (dimethyl sulfoxide) solution containing Ru-sq 5 mg/kg, 10 mg/kg or 15 mg/kg (in volume 200 μ l per 20 g of mouse weight) were administered intraperitoneally to the first three groups (day 1). Another group received cisplatin (5 mg/kg) in the same manner as positive control. The last group (as negative untreated control) received intraperitoneally 5 % solution of DMSO with physiologic solution. The application of all substances was repeated on day 7 of therapy. The animals were observed 60 days from first application, tumor growth, weight of mice and survival were monitored in regular intervals. The mice had free access to water and food ad libitum throughout the experiment. At the end of experiment (after 60 days) all surviving mice were sacrificed by using of overdose of intramuscular anesthetic.

Statistical Analysis for A2780 human ovarian cancer in immunodeficient nude mice.

One-Way Analysis of Variance with post-hoc Dunnetts's multiple comparison test was used to detect differences in tumour weight. Kaplan-Meier curves and logrank tests were used to compare survival times in groups. Here, the level of significance was $\alpha=0.05$. MS Excel 2016 and OriginPro 8 software was used for the calculations and statistical evaluations.

Western Blot analysis of Akt-1 protein levels in HeLa cells.

HeLa cells were seeded on a 10 cm dish so that, at the time of the treatment, cells were confluent. The next day, the cells were treated for 24 h with the compounds. After that time, the cells were collected, counted, snap frozen in liquid nitrogen and then stored at -80 °C. Samples were then lysed in SB buffer in reducing conditions, so that 10 μ L

of the sample contain 100 000 cells. Samples were boiled for 10 min and then passaged five times through 1 mL syringe. Samples were then loaded on 10% SDS-PAGE gels (10 μ L). Proteins were then blotted on a nitrocellulose membrane (Amersham Protran 0.2). Detection of Akt-1 and GAPDH proteins was conducted using following primary antibodies: anti-GAPDH (1:20000 sigma-aldrich G9545) and anti-Akt-1 (B-1) (1:200 Santa Cruz Biotechnology sc-5298). Images were taken using ChemiDoc Touch Imaging System by Biorad. Image with non-saturated bands allowed for normalization in Fiji software.

Associated Content

Supporting Information

The Supporting Information is at DOI: XXXXX.

NMR and HPLC spectra of Ru-sq (Figure S1), crystallographic data of [Ru(DIP)₂(sq)](Cl) (Figure S2), selected bond lengths and angles of Ru-1 molecule (Table S1), selected bond lengths and angles of Ru-2 molecule (Table S2), CV and RDE spectra of Ru-sq (Figure S3), electrochemical data for Ru-sq (Table S3), EPR spectra of Ru-sq (a), its reduced form Ru-sq⁻ (b), and its oxidized form Ru-sq⁺ (c) (Figure S4), overlap of ¹H spectra of Ru-sq in DMSO over 8 days (Figure S5), UV traces of UPLC analysis of Ru-sq (Figure S6a) percentage concentration of Ru-sq over time (Figure S6b), fluorometric cell viability assay (Figure S7), cellTiter Glo® viability Test (Figure S8), cell Death Mechanism (Figure S9), cellular uptake mechanism (Figure S10), oxygen consumption rates and different respiration parameters in HeLa cells (Figure S11), extracellular acidification rate and different parameters of glycolytic respiration in HeLa cells (Figure S12), fuel flex assay in HeLa cells (Figure S13).

Acknowledgements

This work was financially supported by an ERC Consolidator Grant PhotoMedMet to G.G. (GA 681679) and has received support under the program *Investissements d'Avenir* launched by the French Government and implemented by the ANR with the reference ANR-10-IDEX-0001-02 PSL (G.G.). This work was financed by the the Swiss National Science Foundation (Professorships N° PP00P2_133568 and PP00P2_157545 to G.G.), the University of Zurich (G.G), the Novartis Jubilee Foundation (G.G and R.R.), the Forschungskredit of the University of Zurich (R.R.), the UBS Promedica Stiftung (G.G and R.R.) and the Charles University program Progres Q40/01. Ile de France Region is gratefully acknowledged for financial support of 500 MHz NMR spectrometer of Chimie-ParisTech in the framework of the SESAME equipment project. We acknowledge the loan of Agilent's equipment to Chimie ParisTech. Part of this work was supported by IPGP multidisciplinary program PARI and by Region Île-de-France SESAME Grant no. 12015908.

References

- 1 A. Urruticoechea, R. Alemany, J. Balart, A. Villanueva, F. Viñals and G. Capellá, *Curr. Pharm. Des.*, 2010, **16**, 3–10.
- 2 B. B. Rosenberg, *Platin. Met. Rev.*, 1971, **15**, 42–51.
- 3 B. Rosenberg, L. Van Camp and T. Krigas, *Nature*, 1965, **205**, 698–699.
- 4 B. Rosenberg, L. van Camp, E. B. Grimley and A. J. Thomson, *J. Biol. Chem.*, 1967, **242**, 1347–52.
- 5 B. Rosenberg, L. Van Camp, J. E. Trosko and V. H. Mansour, *Nature*, 1969, **222**, 385–386.
- 6 P. Pieter and S. J. Lippard, *Encycl. Cancer*, 1997, **1**, 525–543.
- 7 E. Wong and C. M. Giandomenico, *Chem. Rev.*, 1999, **99**, 2451–2466.
- 8 D. Lebwohl and R. Canetta, *Eur. J. Cancer*, 1998, **34**, 1522–1534.
- 9 S. P. Fricker, *Dalton Trans.*, 2007, **43**, 4903–4917.
- 10 V. Singh, G. K. Azad, A. Reddy M., S. Baranwal and R. S. Tomar, *Eur. J. Pharmacol.*, 2014, **736**, 77–85.
- 11 E. Jamieson and S. Lippard, *Chem. Rev.*, 1999, **99**, 2467–2498.
- 12 M. J. Clarke, F. Zhu and D. R. Frasca, *Chem. Rev.*, 1999, **99**, 2511–2533.
- 13 M. Jakupec, M. Galanski, V. B. Arion, C. G. Hartinger and B. K. Keppler, *Dalton Trans.*, 2008, 183–194.
- 14 P. J. Dyson and G. Sava, *Dalton Trans.*, 2006, 1929–33.
- 15 G. Gasser, I. Ott and N. Metzler-Nolte, *J. Med. Chem.*, 2011, **54**, 3–25.
- 16 T. Gianferrara, I. Bratsos and E. Alessio, *Dalton Trans.*, 2009, 7588–7598.
- 17 B. C. S. Allardyce and P. J. Dyson, *Platin. Met. Rev.*, 2001, **45**, 62–69.
- 18 E. S. Antonarakis and A. Emadi, *Cancer Chemother. Pharmacol.*, 2010, **66**, 1–9.

- 19 M. Pongratz, P. Schluga, M. A. Jakupec, V. B. Arion, C. G. Hartinger, G. Allmaier and B. K. Keppler, *J. Anal. At. Spectrom.*, 2004, **19**, 46–51.
- 20 E. Alessio, *Eur. J. Inorg. Chem.*, 2017, **55**, 1549–1560.
- 21 G. Sava, I. Capozzi, K. Clerici, G. Gagliardi, E. Alessio and G. Mestroni, *Clin. Exp. Metastasis*, 1998, **16**, 371–379.
- 22 F. Lentz, A. Drescher, A. Lindauer, M. Henke, R. a Hilger, C. G. Hartinger, M. E. Scheulen, C. Dittrich, B. K. Keppler and U. Jaehde, *Anticancer. Drugs*, 2009, **20**, 97–103.
- 23 R. Trondl, P. Heffeter, C. R. Kowol, M. a. Jakupec, W. Berger and B. K. Keppler, *Chem. Sci.*, 2014, **5**, 2925–2932.
- 24 C. G. Hartinger, S. Zorbas-Seifried, M. A. Jakupec, B. Kynast, H. Zorbas and B. K. Keppler, *J. Inorg. Biochem.*, 2006, **100**, 891–904.
- 25 H. Yin, J. Roque, P. Konda, S. Monro, K. L. Colo, S. Gujar, R. P. Thummel, L. Lilge, C. G. Cameron and S. A. Mcfarland, *Chem. Rev.*, 2019, **119**, 797–828.
- 26 A. Notaro and G. Gasser, *Chem. Soc. Rev.*, 2017, **46**, 7317–7337.
- 27 C. G. Hartinger, M. a Jakupec, S. Zorbas-Seifried, M. Groessler, A. Egger, W. Berger, H. Zorbas, P. J. Dyson and B. K. Keppler, *Chem. Biodivers.*, 2008, **5**, 2140–2155.
- 28 J. Shum, P. K. Leung and K. K. Lo, *Inorg. Chem.*, 2019, **58**, 2231–2247.
- 29 M. Patra and G. Gasser, *ChemBioChem*, 2012, **13**, 1232–1252.
- 30 M. Dörr and E. Meggers, *Curr. Opin. Chem. Biol.*, 2014, **19**, 76–81.
- 31 M. Jakubaszek, B. Goud and S. Ferrari, 2018, 13040–13059.
- 32 M. R. Gill, H. Derrat, C. G. W. Smythe, G. Battaglia and J. A. Thomas, *ChemBioChem*, 2011, **12**, 877–880.
- 33 N. Deepika, C. Shobha Devi, Y. Praveen Kumar, K. Laxma Reddy, P. Venkat Reddy, D. Anil Kumar, S. S. Singh and S. Satyanarayana, *J. Photochem. Photobiol. B Biol.*, 2016, **160**, 142–153.

- 34 H. Wang, Y. Liu, M. Li, H. Huang, H. M. Xu, R. J. Hong and H. Shen, *Dalt. Trans.*, 2013, **42**, 4386–4397.
- 35 A. Srishailam, Y. P. Kumar, P. Venkat Reddy, N. Nambigari, U. Vuruputuri, S. S. Singh and S. Satyanarayana, *J. Photochem. Photobiol. B Biol.*, 2014, **132**, 111–123.
- 36 C. Tan, S. Lai, S. Wu, S. Hu, L. Zhou, Y. Chen, M. Wang, Y. Zhu, W. Lian, W. Peng, L. Ji and A. Xu, *J. Med. Chem.*, 2010, **53**, 7613–7624.
- 37 V. Pierroz, T. Joshi, A. Leonidova, C. Mari, J. Schur, I. Ott, L. Spiccia, S. Ferrari and G. Gasser, *J. Am. Chem. Soc.*, 2012, **134**, 20376–20387.
- 38 G. Bin Jiang, X. Zheng, J. H. Yao, B. J. Han, W. Li, J. Wang, H. L. Huang and Y. J. Liu, *J. Inorg. Biochem.*, 2014, **141**, 170–179.
- 39 Y. C. Wang, C. Qian, Z. L. Peng, X. J. Hou, L. L. Wang, H. Chao and L. N. Ji, *J. Inorg. Biochem.*, 2014, **130**, 15–27.
- 40 J. F. Kou, C. Qian, J. Q. Wang, X. Chen, L. L. Wang, H. Chao and L. N. Ji, *J. Biol. Inorg. Chem.*, 2012, **17**, 81–96.
- 41 U. Schatzschneider, J. Niesel, I. Ott, R. Gust, H. Alborzinia and S. Wölfel, *ChemMedChem*, 2008, **3**, 1104–1109.
- 42 M. D. Ward, J. A. McCleverty and M. D. Ward, *J. chem. soc. Dalt. Trans.*, 2002, 275–288.
- 43 A. Vlček, *Comments Inorg. Chem.*, 1994, **16**, 207–228.
- 44 C. G. Pierpont, *Coord. Chem. Rev.*, 2001, **217**, 99–125.
- 45 C. Creutz, *Prog. Inorg. Chem.*, 1983, **30**, 1–73.
- 46 M. Haga, E. S. Dodsworth and A. B. P. Lever, *Inorg. Chem.*, 1986, **25**, 447–453.
- 47 T. Wada, M. Yamanaka, T. Fujihara, Y. Miyazato and K. Tanaka, *Inorg. Chem.*, 2006, **45**, 8887–8894.
- 48 J. T. Muckerman, D. E. Polyansky, T. Wada, K. Tanaka and E. Fujita, *Inorg. Chem.*, 2008, **47**, 1787–1802.

- 49 S. E. Jones, D. Chin and D. T. Sawyer, *Inorg Chem*, 1981, **20**, 4257–4262.
- 50 J. B. Baell, *J. Nat. Prod.*, 2016, **79**, 616–628.
- 51 R. M. F. Lima, L. D. G. Alvarez, M. F. D. Costa, S. L. Costa and R. S. El-bachá, *Gen. Physiol. Biophys*, 2008, **27**, 306–314.
- 52 W. L. C. Almeida, D. N. Vítor, M. R. G. Pereira, D. S. De Sá, L. D. G. Alvarez, A. M. Pinheiro, S. L. Costa, M. F. D. Costa, Z. N. Da Rocha and R. S. El-Bachá, *J. Chil. Chem. Soc.*, 2007, **52**, 1240–1243.
- 53 D. Lin, F. Dai, L. Di Sun and B. Zhou, *Mol. Nutr. Food Res.*, 2015, **59**, 2395–2406.
- 54 R. Galvao de Lima, A. B. P. Lever, I. Y. Ito and R. Santana da Silva, *Transit. Met. Chem.* 28, 2003, **28**, 272–275.
- 55 V. T. Huong, T. Shimanouchi, N. Shimauchi, H. Yagi, H. Umakoshi, Y. Goto and R. Kuboi, *J. Biosci. Bioeng.*, 2010, **109**, 629–634.
- 56 A. L. and P. A. L. Debbie C. Crans, Jordan T. Koehn, Stephanie M. Petry, Caleb M. Glover, Asanka Wijetunga Ravinder Kaur, *Dalt. Trans.*, 2019, **48**, 6383–6395.
- 57 D. C. C. and M. D. J. Brant G. Lemons, David T. Richens, Ashley Anderson, Myles Sedgwick, *New J. Chem*, 2013, **37**, 75–91.
- 58 I. Brastos, E. Alessio, M. E. Ringenberg and T. B. Rauchfuss, *Inorg. Synth.*, 2010, **35**, 148–163.
- 59 R. Caspar, C. Cordier, J. B. Waern, C. Guyard-Duhayon, M. Gruselle, P. Le Floch and H. Amouri, *Inorg. Chem.*, 2006, **45**, 4071–4078.
- 60 O. Carugo, C. B. Castellani, K. Djinovicb and M. Rizzi, *J. CHEM. SOC. Dalt. TRANS*, 1992, **10**, 1–5.
- 61 S. L. H. Higgins, T. A. White, B. S. J. Winkel and K. J. Brewer, *Inorg. Chem.*, 2011, **50**, 463–470.
- 62 M. T. Mongelli and K. J. Brewer, *Inorg. Chem. Commun.*, 2006, **9**, 877–881.

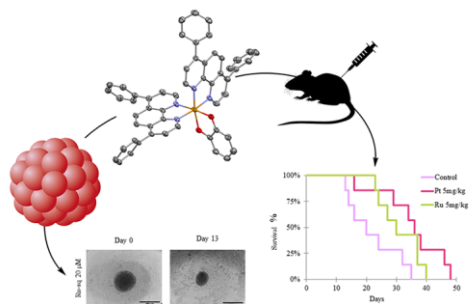
- 63 O. K. Medhi and U. Agarwala, *Inorg Chem*, 1980, **1**, 1381–1384.
- 64 N. G. Connelly and W. E. Geiger, *Chem. Rev.*, 1996, **96**, 877–910.
- 65 D. Bao, B. Millare, W. Xia, B. G. Steyer, A. A. Gerasimenko, A. Ferreira, A. Contreras and V. I. Vullev, *J. Phys. Chem. A*, 2009, **2**, 1259–1267.
- 66 A. Frei, R. Rubbiani, S. Tubafard, O. Blacque, P. Anstaett, A. Felgenträger, T. Maisch, L. Spiccia and G. Gasser, *J. Med. Chem.*, 2014, **57**, 7280–7292.
- 67 V. Cepeda, M. Fuertes, J. Castilla, C. Alonso, C. Quevedo and J. Perez, *Anticancer. Agents Med. Chem.*, 2007, **7**, 3–18.
- 68 H. G. Keizer, H. M. Pinedo, G. J. Schuurhuis and H. Joenje, *Pharmac. Ther.*, 1990, **47**, 219–231.
- 69 J. M. Kelm, N. E. Timmins, C. J. Brown, M. Fussenegger and L. K. Nielsen, *Biotechnol. Bioeng.*, 2003, **83**, 173–180.
- 70 H. Ma, Q. Jiang, S. Han, Y. Wu, J. C. Tomshine, D. Wang, Y. Gan and G. Zou, *Mol. Imaging*, 2012, **11**, 487–498.
- 71 M. Kapałczyńska, T. Kolenda, A. Przybyła, Weronika Zajączkowska, Maria Teresiak, V. Filas, M. Ibbs, R. Bliźniak and K. Łuczewski, Łukasz Lamperska, *Arch Med Sci*, 2018, **4**, 910–919.
- 72 J. Friedrich, C. Seidel, R. Ebner and L. A. Kunz-schughart, *Nat. Protoc.*, 2009, **4**, 309–324.
- 73 J. Hess, H. Huang, A. Kaiser, V. Pierroz and O. Blacque, 2017, 9888–9896.
- 74 O. W. Seo, M. Kim, J. Hulme and S. S. A. An, 2016, 7207–7218.
- 75 A. M. Rieger, K. L. Nelson, J. D. Konowalchuk and D. R. Barreda, *J. Vis. Exp.*, 2011, 2–5.
- 76 Â. A. Belmokhtar, J. Hillion and E. Se, 2001, 3354–3362.
- 77 C. A. Puckett and J. K. Barton, *J. Am. Chem. Soc.*, 2009, **131**, 8738–8739.
- 78 B. M. Goldstein, J. K. Barton and H. M. Berman, *Inorg. Chem.*, 1986, **25**, 842–

- 847.
- 79 Y. Tsujimoto and Osaka, 2000, 134–135.
- 80 V. N. Dedov, G. C. Cox and B. D. Roufogalis, *Micron*, 2001, **32**, 653–660.
- 81 L. Zhuang and X. L. and W. H. Huanjie Wei, Qing Li, Xianlong Su, Shujuan Liu, Kenneth Yin Zhang, Wen Lv, Qiang Zhao, *Chem. Sci.*, 2018, **9**, 502–512.
- 82 L. D. Zorova, V. A. Popkov, E. Y. Plotnikov, D. N. Silachev, B. Pevzner, S. S. Jankauskas, V. A. Babenko, S. D. Zorov, A. V Balakireva, M. Juhaszova, S. J. Sollott and D. B. Zorov, *Anal. Biochem.*, 2018, 50–59.
- 83 J. D. Ly, D. R. Grubb and A. Lawen, *Apoptosis*, 2003, **8**, 115–128.
- 84 S. Sakamuru, M. S. Attene-ramos and M. Xia, in *High-Throughput Screening Assays in Toxicology, Methods in Molecular Biology*, 2016, vol. 1473, pp. 17–22.
- 85 L. Zhen-ge, R. Xiao-hua, W. Sha-sha, L. Xin-hua and T. Ya-ling, *Onco. Targets. Ther.*, 2016, **9**, 545–555.
- 86 J. Jung, *Toxicol. Res.*, 2014, **30**, 1–5.
- 87 C. Xu, X. Li, P. Liu, M. A. N. Li and F. Luo, *Oncol. Lett.*, 2019, **5**, 3–10.
- 88 A. S. Clark, K. West, S. Streicher and P. A. Dennis, *Mol. Cancer Ther.*, 2002, **1**, 707–717.
- 89 J. U. N. Zhang, L. L. I. Zhang, L. E. I. Shen, X. Xu and H. G. Yu, *Oncol. Lett.*, 2013, **5**, 756–760.
- 90 S. A. Santi, A. C. H. Douglas and Lee, *BioMol Concepts*, 2010, **1**, 389–401.
- 91 G. R. Fulmer, A. J. M. Miller, N. H. Sherden, H. E. Gottlieb, A. Nudelman, B. M. Stoltz, J. E. Bercaw and K. I. Goldberg, *Organometallics*, 2010, **29**, 2176–2179.
- 92 M. Krachler, *J. Environ. Monit.*, 2007, **9**, 790–804.
- 93 *Rigaku Oxford Diffraction*, 2015.

- 94 R. C. Clark and J. S. Reid, *Acta Crystallogr. Sect. A*, 1995, **51**, 887–897.
- 95 *CrysAlisPro (version 1.171.39.9f)*, Rigaku Oxford Diffraction, 2015.
- 96 O. V. Dolomanov, L. J. Bourhis, R. J. Gildea, J. A. K. Howard and H. Puschmann, *J. Appl. Cryst.*, 2009, **42**, 339.
- 97 G. M. Sheldrick, *Acta Crystallogr. Sect. A Found. Crystallogr.*, 2015, **71**, 3–8.
- 98 G. M. Sheldrick, *Acta Crystallogr. Sect. C Struct. Chem.*, 2015, **71**, 3–8.
- 99 A. L. Spek, *J. Appl. Crystallogr.*, 2003, **36**, 7–13.
- 100 S. Stoll and A. Schweiger, *J. Magn. Reson.*, 2006, **178**, 42–55.
- 101 J. Karges, U. Basu, O. Blacque, H. Chao and G. Gasser, *Angew. Chemie Int. Ed.*,
, DOI:10.1002/anie.201907856.
- 102 M. Tharaud, S. Gardoll, O. Khelifi, M. F. Benedetti and Y. Sivry, *Microchem. J.*, 2015, **121**, 32–40.

Table of content

A ruthenium (II) polypyridyl complex bearing a non-innocent dioxo ligand demonstrates an impressive potential as a chemotherapeutic agent against cancer both *in vitro* and *in vivo*.



Supplementary Information

A Ruthenium(II) Complex Containing a Redox-Active Semiquinonate Ligand as Potential Chemotherapeutic Agent: From synthesis to *in vivo* Studies

Anna Notaro,^{a,#} Angelo Frei,^{b,#} Riccardo Rubbiani,^{b,#} Marta Jakubaszek,^{a, e} Uttara Basu,^a Severin Koch,^b Cristina Mari,^b Mazzarine Dotou,^a Olivier Blacque,^b Jérémie Gouyon,^c Fethi Bedioui,^c Nils Rotthowe,^d Rainer F. Winter,^d Bruno Goud,^e Stefano Ferrari,^f Mickaël Tharaud,^g Martina Řezáčová,^h Jana Humajová,ⁱ Pavel Tomšík,^h and Gilles Gasser^{a,}*

^a Chimie ParisTech, PSL University, CNRS, Institute of Chemistry for Life and Health Sciences, Laboratory for Inorganic Chemical Biology, F-75005 Paris, France.

^b Department of Chemistry, University of Zurich, Winterthurerstrasse 190, 8057 Zurich, Switzerland.

^c Chimie ParisTech, PSL University, CNRS, Institute of Chemistry for Life and Health Sciences, Team Synthèse, Electrochimie, Imagerie et Systèmes Analytiques pour le Diagnostic, F-75005 Paris, France.

^d Department of Chemistry, University of Konstanz, Universitätsstrasse 10, D-78457 Konstanz, Germany.

^e Institut Curie, PSL University, CNRS UMR 144, Paris, France.

^f Institute of Molecular Cancer Research, University of Zurich, Zurich, Switzerland.

^g Université de Paris, Institut de physique du globe de Paris, CNRS, F-75005 Paris, France.

^h Department of Medical Biochemistry, Faculty of Medicine in Hradec Kralove, Charles University, Czech Republic.

ⁱ Department of Medical Biochemistry, Faculty of Medicine in Prague, Czech Republic.

these authors have contributed equally to the work

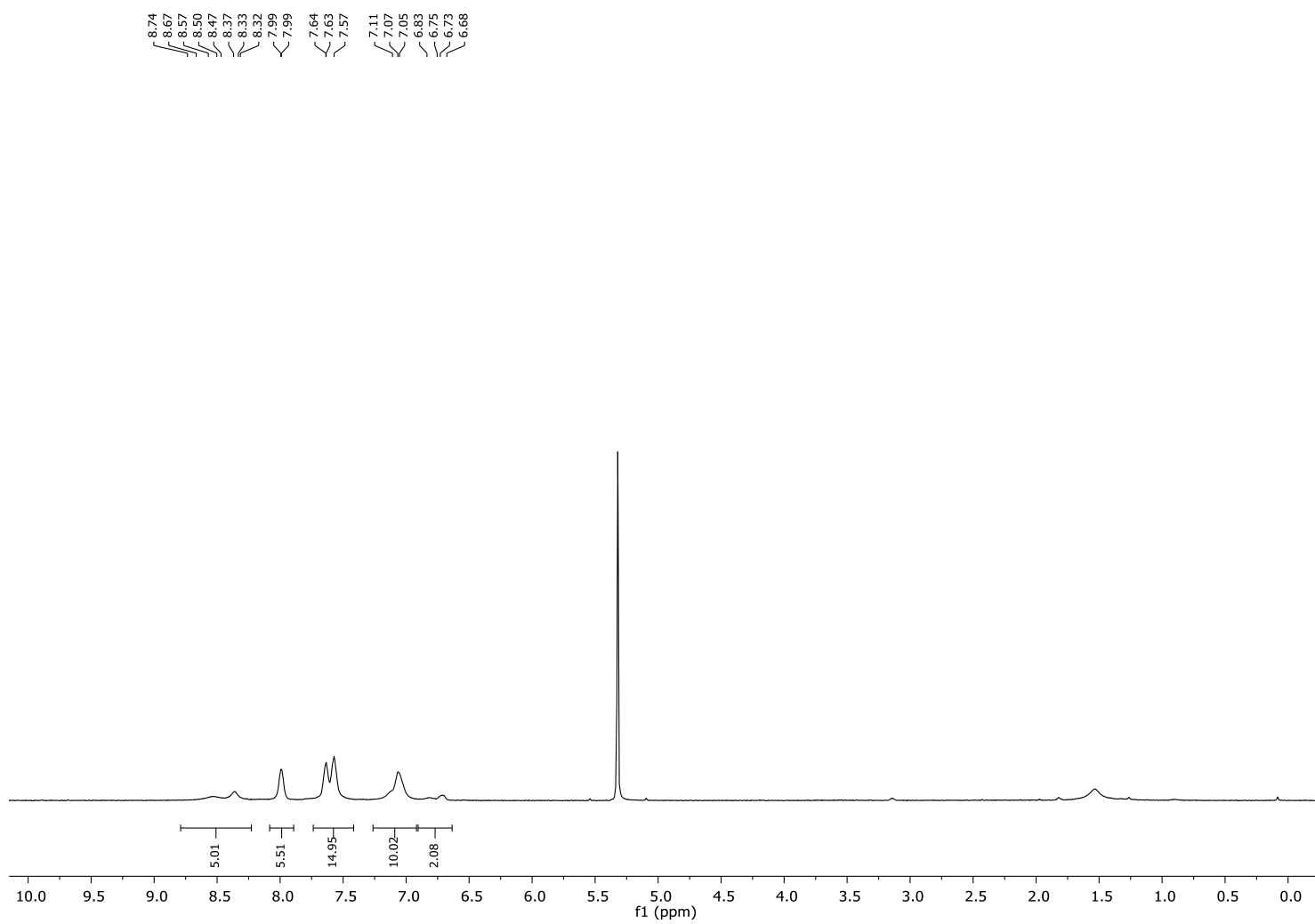
* Corresponding author: E-mail: gilles.gasser@chimeparistech.psl.eu; WWW: www.gassergroup.com;
Phone: +33 1 44 27 56 02

Table of Contents

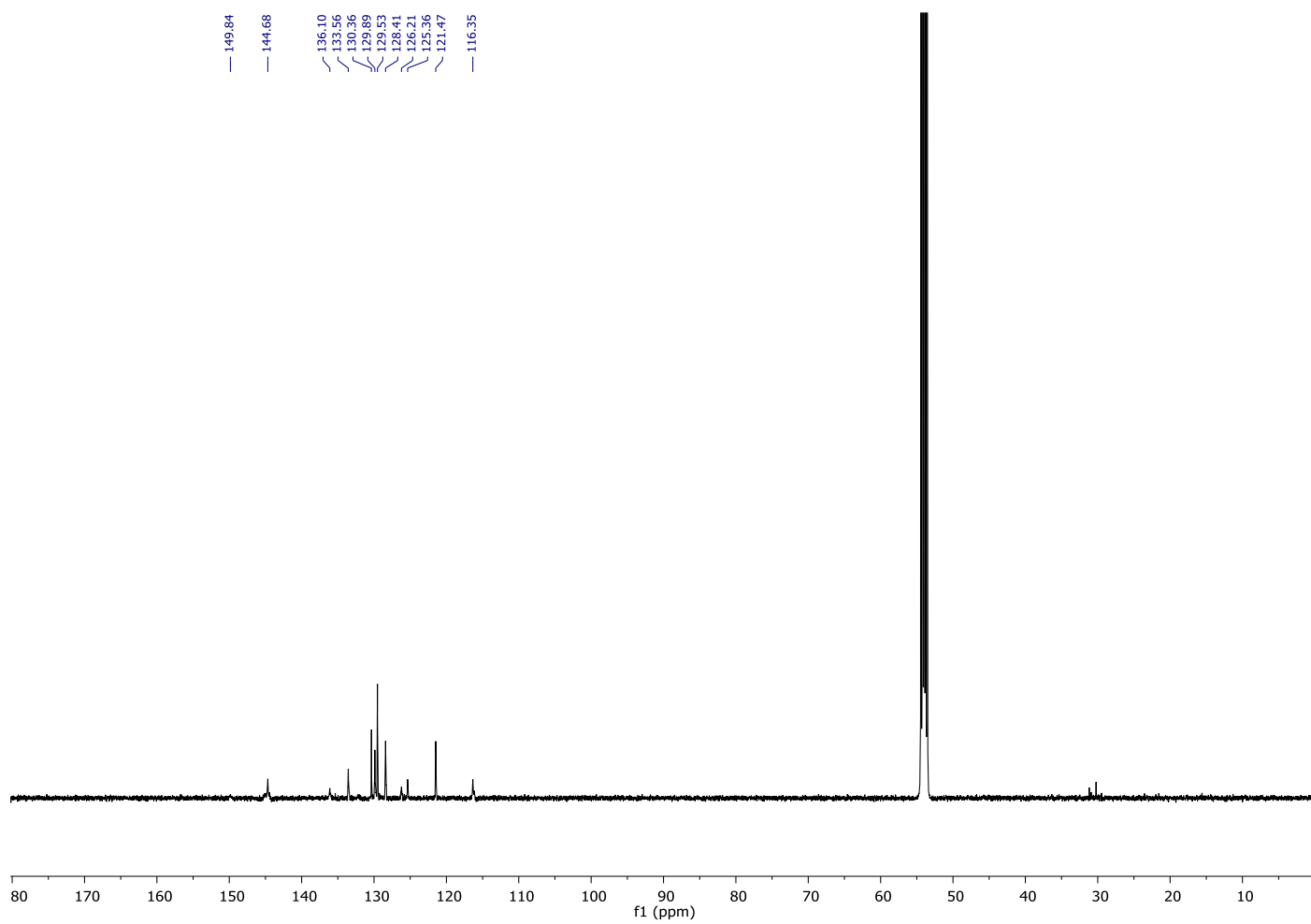
1) Figure S1. NMR and HPLC spectra of Ru-sq	3
2) Figure S2. Crystallographic data of [Ru(DIP)₂(sq)](Cl)	6
3) Table S1. Selected bond lengths and angles of Ru-1 molecule.....	7
4) Table S2. Selected bond lengths and angles of Ru-2 molecule.....	7
5) Figure S3. CV and RDE spectra of Ru-sq	8
6) Table S3. Electrochemical data for Ru-sq	9
7) Figure S4. EPR spectra of Ru-sq (a), its reduced for Ru-sq⁻ (b), and its oxidized form Ru-sq⁺ (c)...	10
8) Figure S5. Overlap of ¹ H spectra of Ru-sq in DMSO over 8 days.....	11
9) Figure S6. a) UV traces of UPLC analysis of Ru-sq b) Percentage concentration of Ru-sq over time.....	12
10) Figure S7. Fluorometric cell viability assay.....	13
11) Figure S8. CellTiter Glo [®] viability Test.....	19
12) Figure S9. Cell Death Mechanism.....	20
13) Figure S10. Cellular uptake mechanism	21
14) Figure S11. Oxygen consumption rates and different respiration parameters in HeLa cells.....	22
15) Figure S12. Extracellular acidification rate and different parameters of glycolytic respiration in HeLa cells.....	23
16) Figure S13. Fuel flex assay in HeLa cells.....	24

1) Figure S1. NMR and HPLC spectra of Ru-sq.

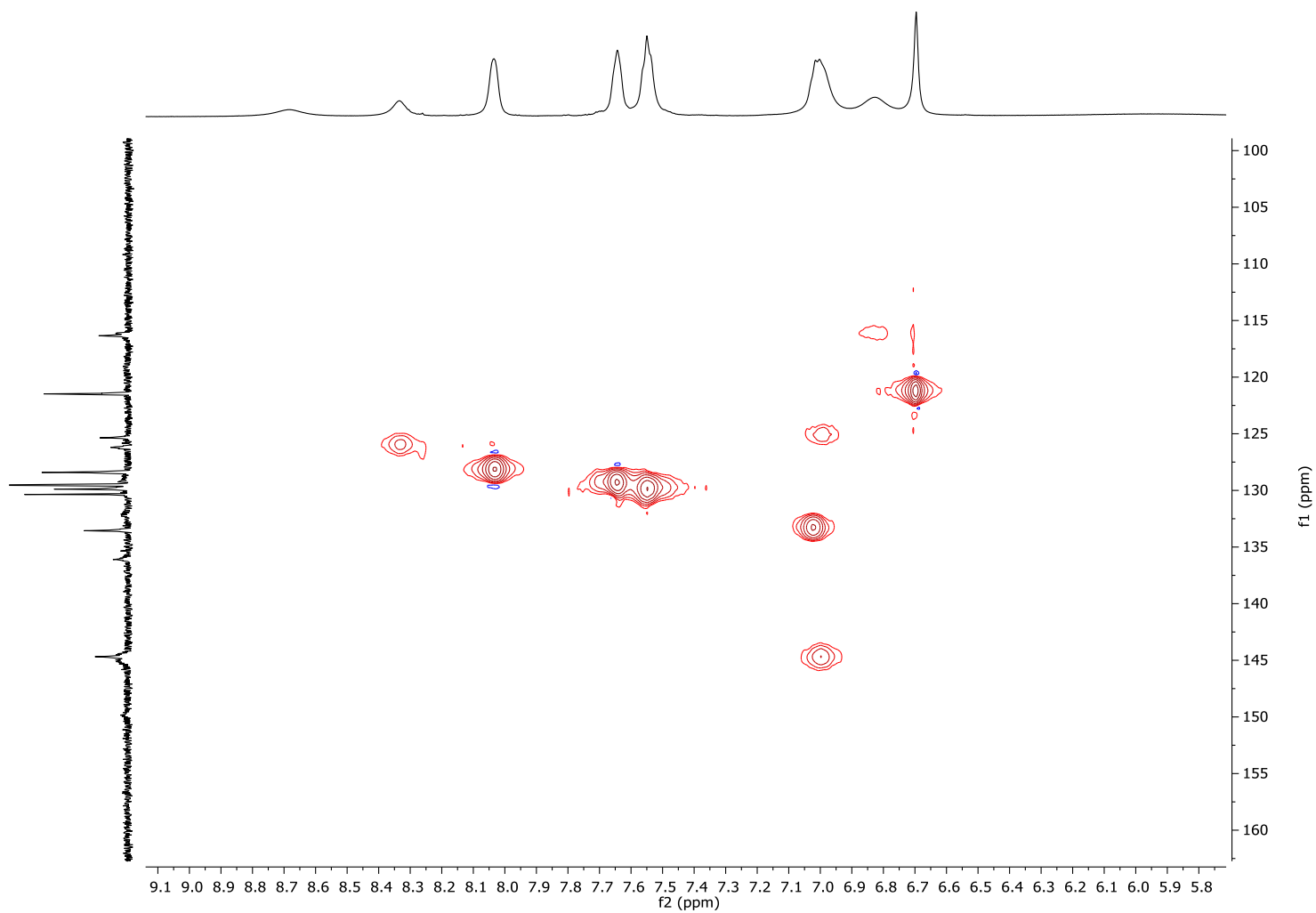
Ru-sq, ^1H , CD_2Cl_2 , 400 MHz



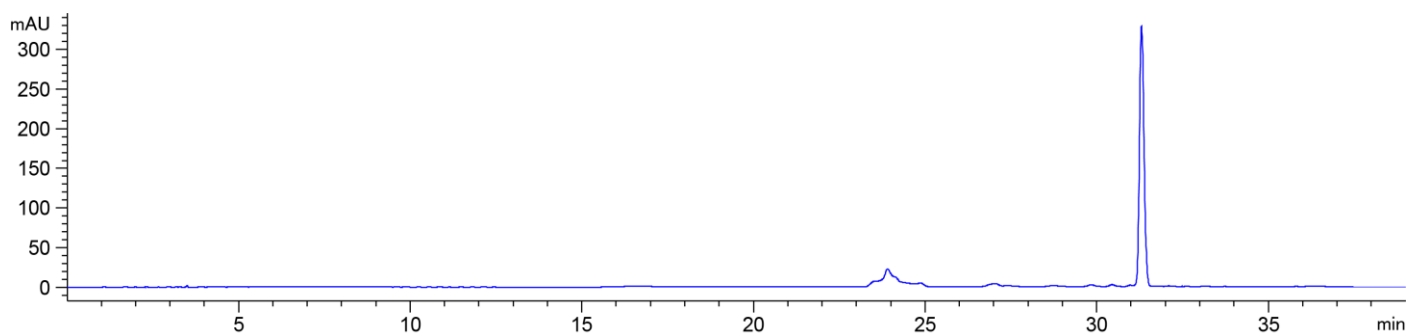
Ru-sq, ^{13}C , CD_2Cl_2 , 125 MHz



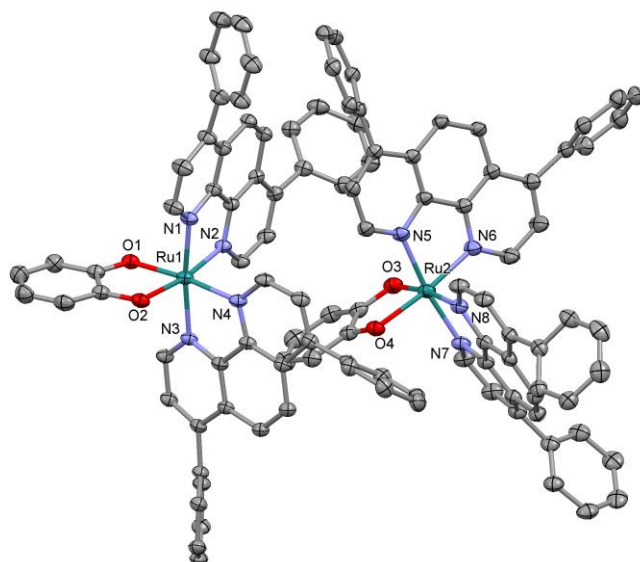
Ru-sq, 2D ^1H - ^{13}C HSQC, CD_2Cl_2 , 125 MHz



Ru-sq, HPLC trace recorded at 450nm



2) Figure S2. Crystallographic data of [Ru(DIP)₂(sq)](Cl).



Empirical formula	C ₁₀₈ H ₇₈ Cl ₂ N ₈ O ₇ Ru ₂
Formula weight	1872.82
Temperature/K	183(1)
Crystal system	monoclinic
Space group	P2 ₁ /c
a/Å	14.31140(10)
b/Å	23.42500(10)
c/Å	25.4275(2)
α/°	90
β/°	93.0470(10)
γ/°	90
Volume/Å ³	8512.38(10)
Z	4
ρ _{calc} /cm ³	1.457
μ/mm ⁻¹	3.983
F(000)	4324.0
Crystal size/mm ³	0.22 × 0.03 × 0.02
Radiation	Cu Kα (λ = 1.54184)
2θ range for data collection/°	5.132 to 149.008
Index ranges	-17 ≤ h ≤ 16, -29 ≤ k ≤ 20, -29 ≤ l ≤ 31
Reflections collected	74910
Independent reflections	17374 [R _{int} = 0.0425, R _{sigma} = 0.0339]
Data/restraints/parameters	17374/0/1161
Goodness-of-fit on F ²	1.031
Final R indexes [I ≥ 2σ (I)]	R ₁ = 0.0462, wR ₂ = 0.1187
Final R indexes [all data]	R ₁ = 0.0530, wR ₂ = 0.1237
Largest diff. peak/hole / e Å ⁻³	1.35/-0.79

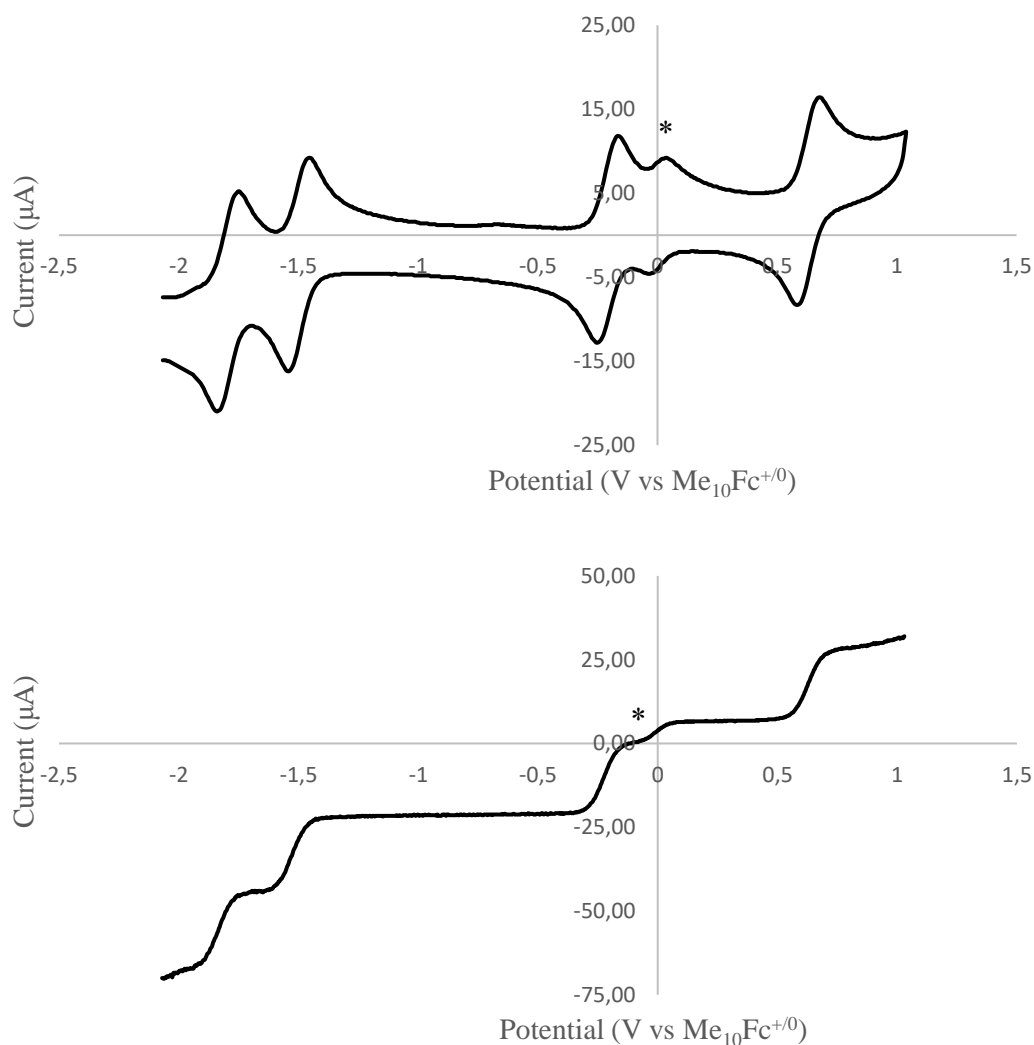
3) Table S1. Selected bond lengths and angles of **Ru-1** molecule.

Bond Atoms	Bond Length [Å]	Angle Atoms	Bond Angle [°]
Ru1-N1	2.052(2)	N1-Ru1-N2	79.72(10)
Ru1-N2	2.044(3)	N2-Ru1-N3	98.36(10)
Ru1-N3	2.067(2)	N3-Ru1-N1	172.13(11)
Ru1-N4	2.052(3)	N2-Ru1-N4	90.85(10)
Ru1-O1	2.033(2)	O1-Ru1-N1	92.97(10)
Ru1-O2	2.054(2)	O2-Ru1-N3	89.05(9)
O1-C1	1.309(4)	O1-Ru1-O2	81.03(9)
O2-C2	1.315(4)		

4) Table S2. Selected bond lengths and angles of **Ru-2** molecule.

Bond Atoms	Bond Length [Å]	Angle Atoms	Bond Angle [°]
Ru2-N5	2.067(3)	N5-Ru2-N6	79.68(11)
Ru2-N6	2.047(3)	N6-Ru2-N7	93.54(11)
Ru2-N7	2.058(3)	N7-Ru2-N5	171.19(12)
Ru2-N8	2.058(3)	N6-Ru2-N8	92.31(12)
Ru2-O3	2.035(3)	O3-Ru2-N5	92.21(11)
Ru2-O4	2.031(3)	O4-Ru2-N7	91.37(10)
O3-C55	1.319(4)	O3-Ru2-O4	81.19(10)
O4-C56	1.314(4)		

5) Figure S3. CV and RDE voltammograms of **Ru-sq** (from -2.1 to +1 V) at a glassy carbon electrode in DMF (1 mM) containing Bu₄NPF₆ (100 mM) as supporting electrolyte and decamethylferrocene as an internal standard (0.25 mM) versus calomel. Data were recorded versus saturated calomel electrode at scan rate of 100 mV/s and recalculated versus Me₁₀Fc^{0/+} potential value (feature marked with * in Figure S2).



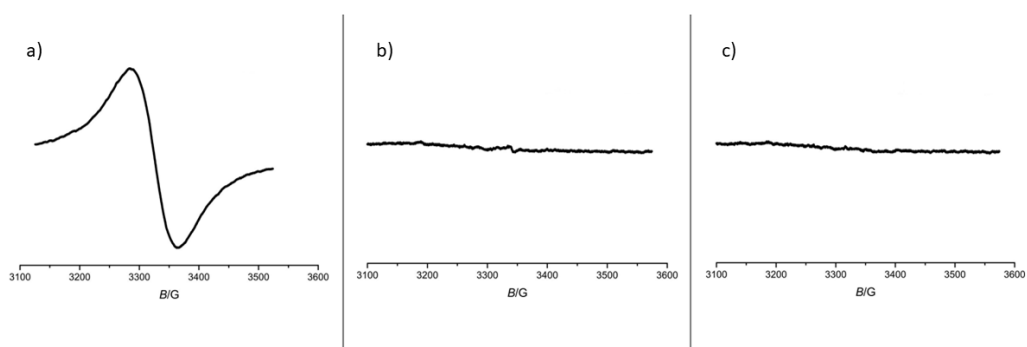
6) Table S3. Electrochemical data for **Ru-sq**.

		DIP^{0/-}	DIP^{0/-}	Sq/cat	Ru^{II/III}
Ru-sq	E_{1/2}^a [V] (RDE)	-1.876 ± 0.039	-1.578 ± 0.035	-0.249 ± 0.010	0.647 ± 0.018
	E_{1/2}^b [V] (CV)	-1.816 ± 0.015	-1.507 ± 0.007	-0.209 ± 0.002	0.623 ± 0.005

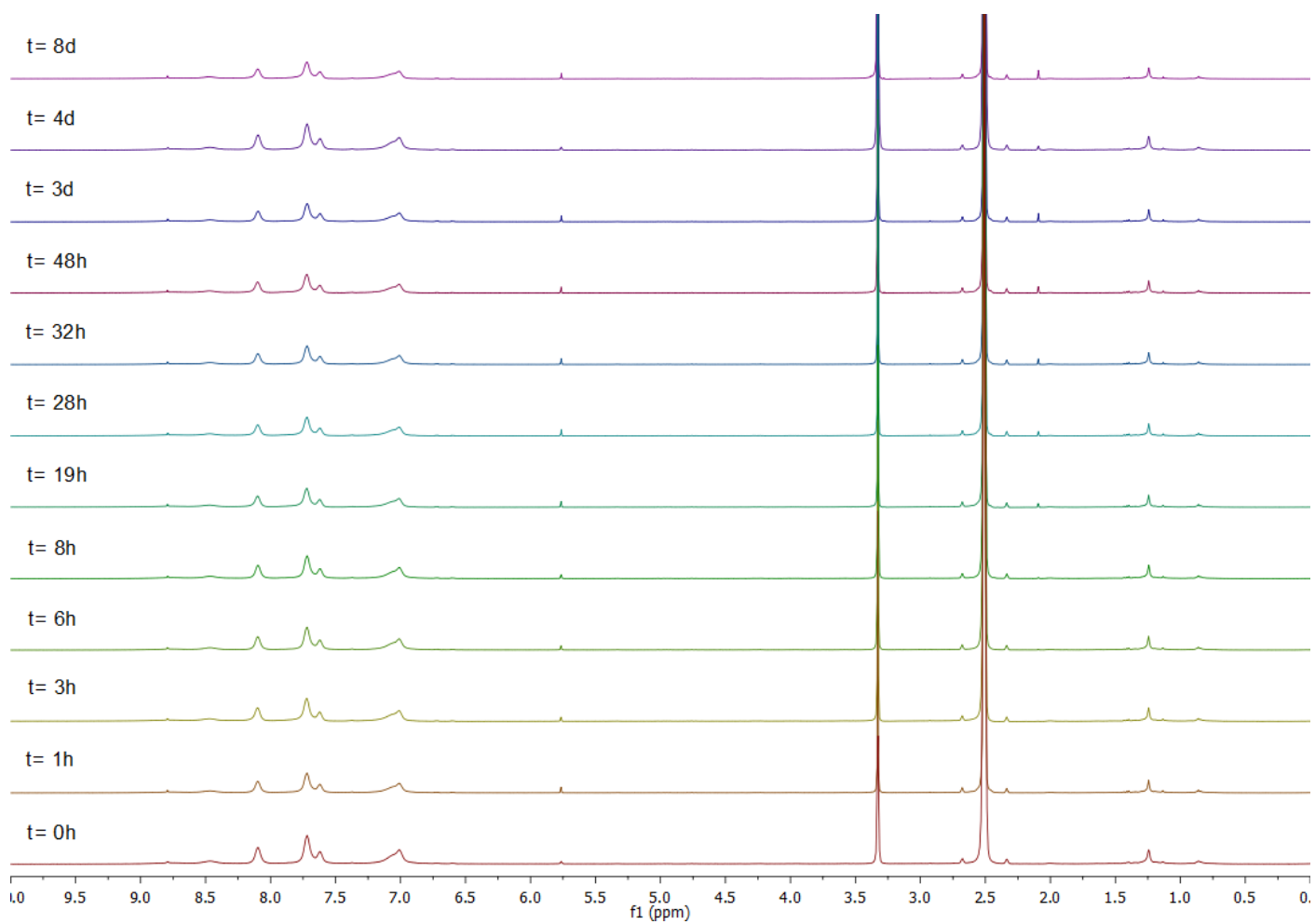
^a E_{1/2} = half-wave.

^b E_{1/2} = (E_{pa} + E_{pc})/2.

7) **Figure S4.** EPR spectra of **Ru-sq** (a), its reduced for **Ru-cat** (b), and its oxidized form **Ru-q** (c).

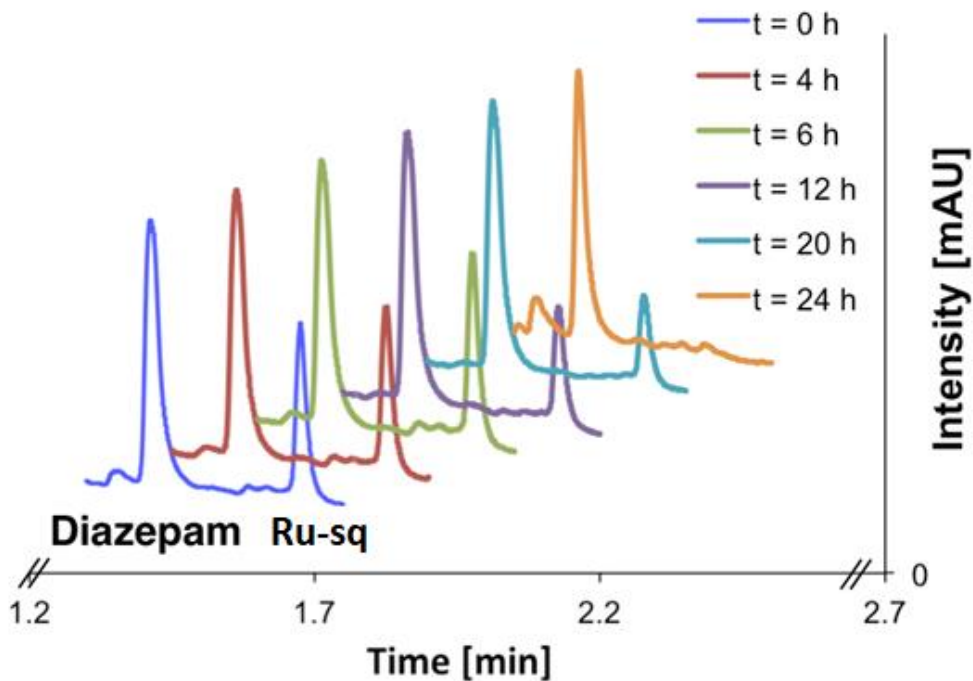


8) **Figure S5.** Overlap of ^1H spectra of **Ru-sq** in DMSO over 8 days.

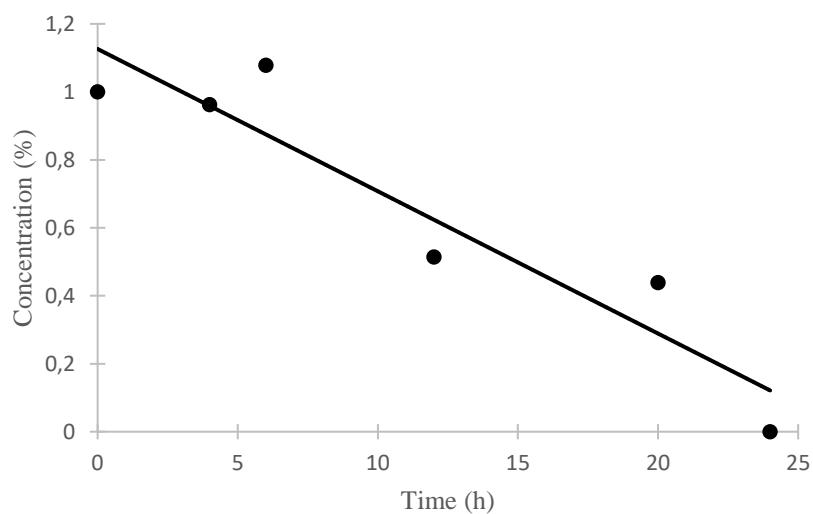


9) **Figure S6.** a) UV traces of UPLC analysis of **Ru-sq** incubated in human plasma at 37 °C for 0 h, 4 h, 6 h, 12 h, 20 h and 24 h using diazepam as an internal standard. b) Percentage concentration of **Ru-sq**, normalized with respect to the internal standard and plotted against time.

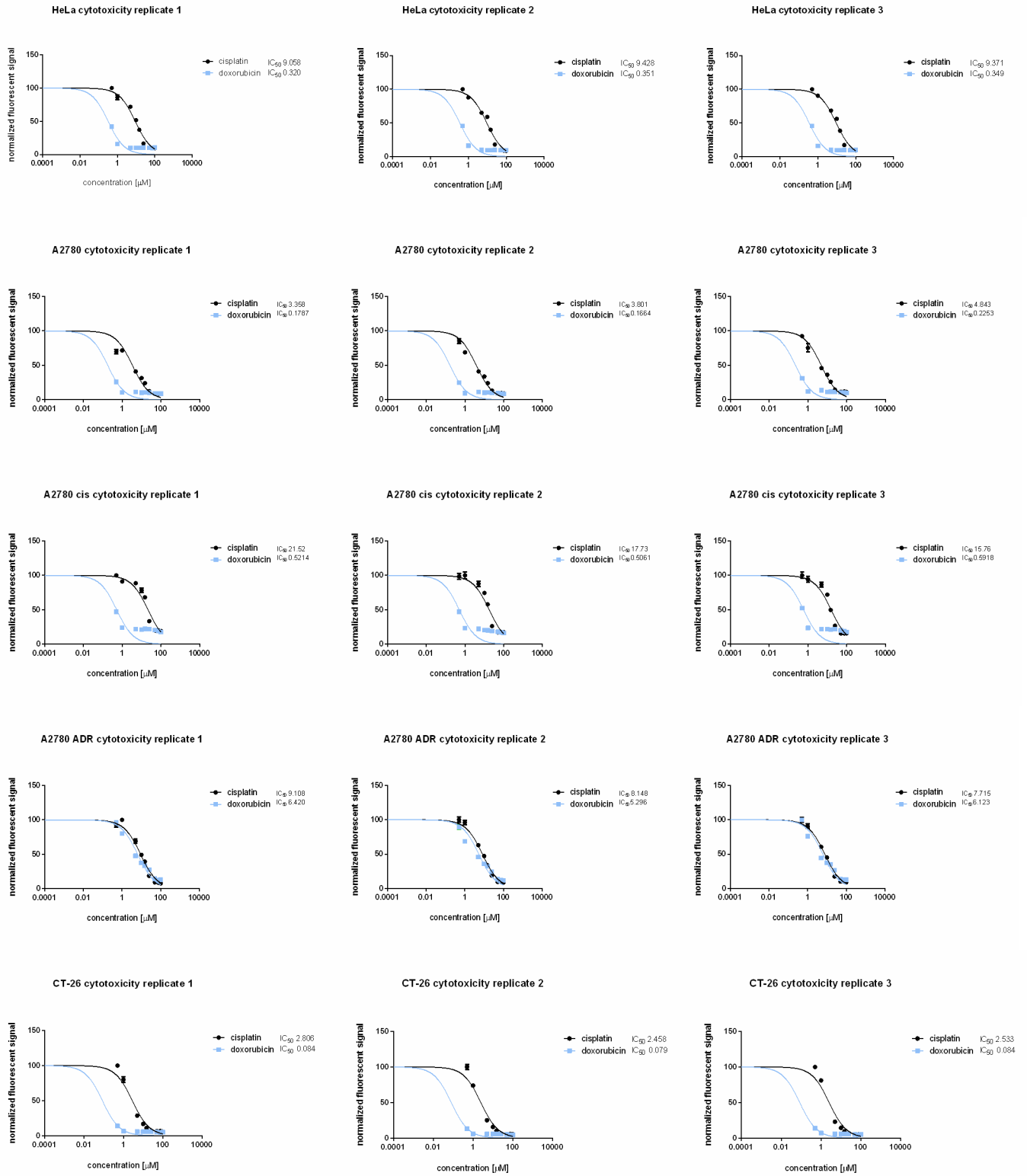
a)



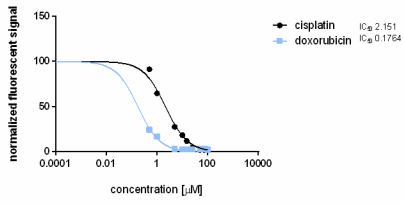
b)



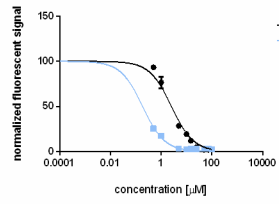
10) Figure S7. Fluorometric cell viability assay.



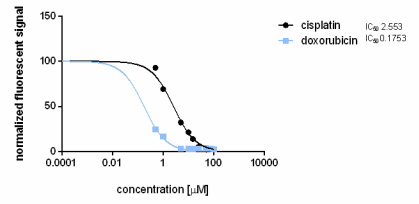
CT-26 LUC cytotoxicity replicate 1



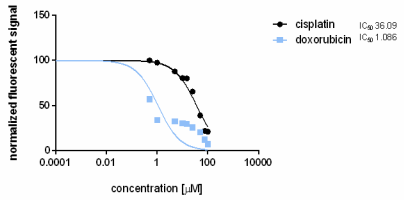
CT-26 LUC cytotoxicity replicate 2



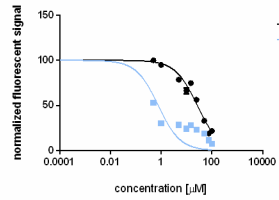
CT-26 LUC cytotoxicity replicate 3



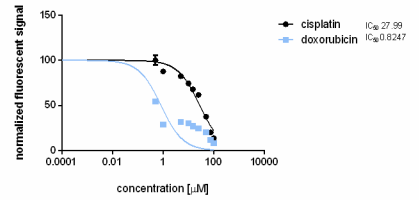
RPE-1 cytotoxicity replicate 1



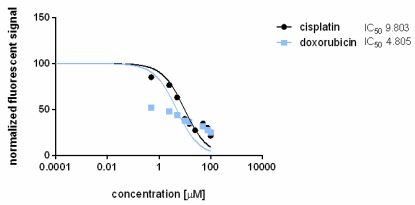
RPE-1 cytotoxicity replicate 2



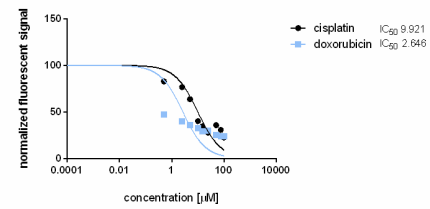
RPE-1 cytotoxicity replicate 3



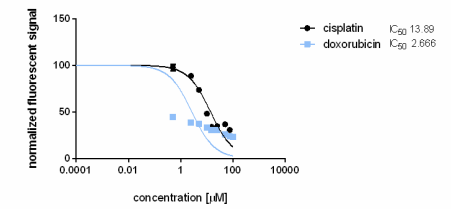
MRC-5 cytotoxicity replicate 1



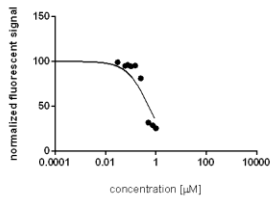
MRC-5 cytotoxicity replicate 2



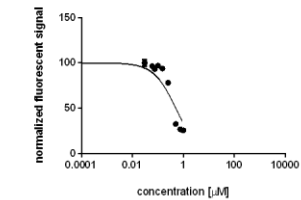
MRC-5 cytotoxicity replicate 3



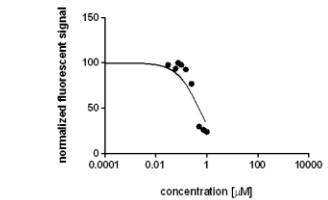
HeLa cytotoxicity replicate 1



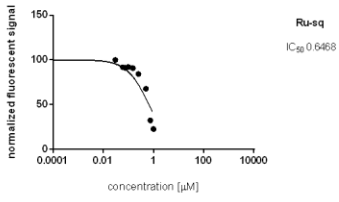
HeLa cytotoxicity replicate 2



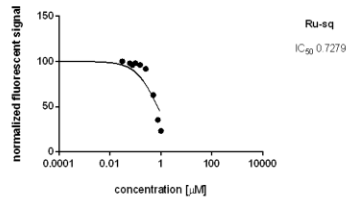
HeLa cytotoxicity replicate 3



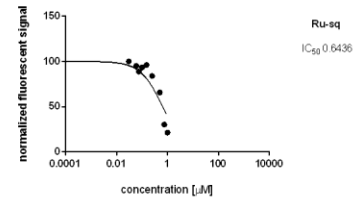
A2780 cytotoxicity replicate 1



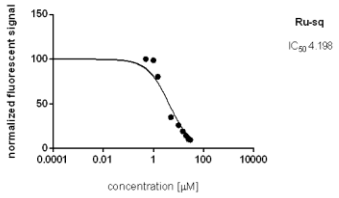
A2780 cytotoxicity replicate 2



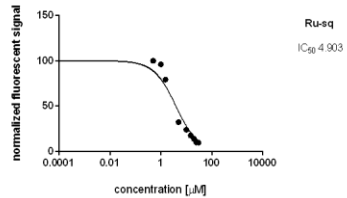
A2780 cytotoxicity replicate 3



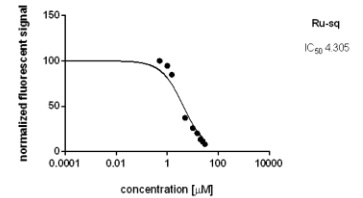
A2780 ADR cytotoxicity replicate 1



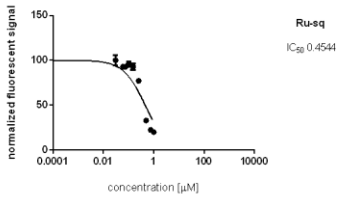
A2780 ADR cytotoxicity replicate 2



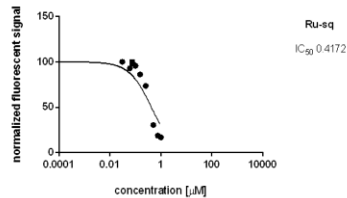
A2780 ADR cytotoxicity replicate 3



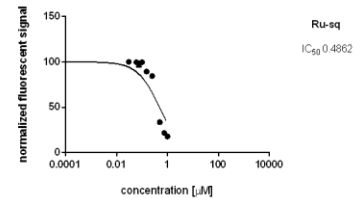
A2780 cis cytotoxicity replicate 1



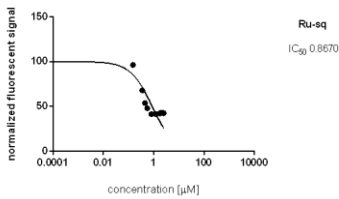
A2780 cis cytotoxicity replicate 2



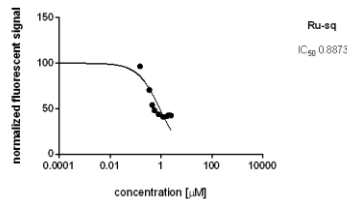
A2780 cis cytotoxicity replicate 3



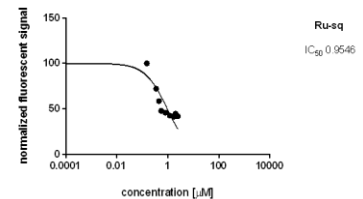
CT-26 cytotoxicity replicate 1



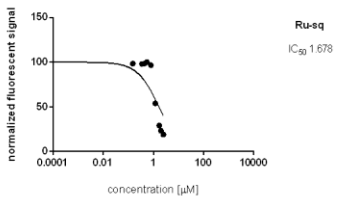
CT-26 cytotoxicity replicate 2



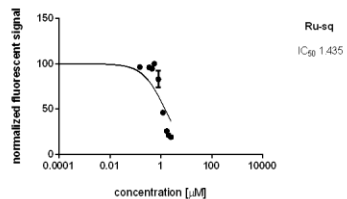
CT-26 cytotoxicity replicate 3



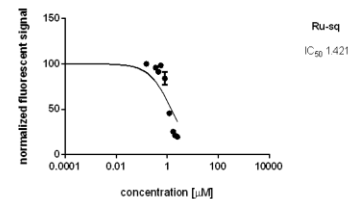
CT-26 LUC cytotoxicity replicate 1



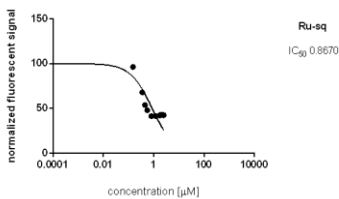
CT-26 LUC cytotoxicity replicate 2



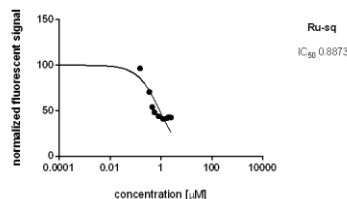
CT-26 LUC cytotoxicity replicate 3



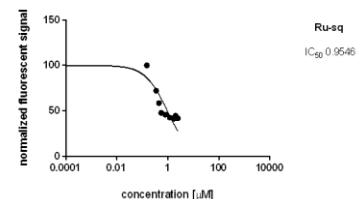
RPE-1 cytotoxicity replicate 1

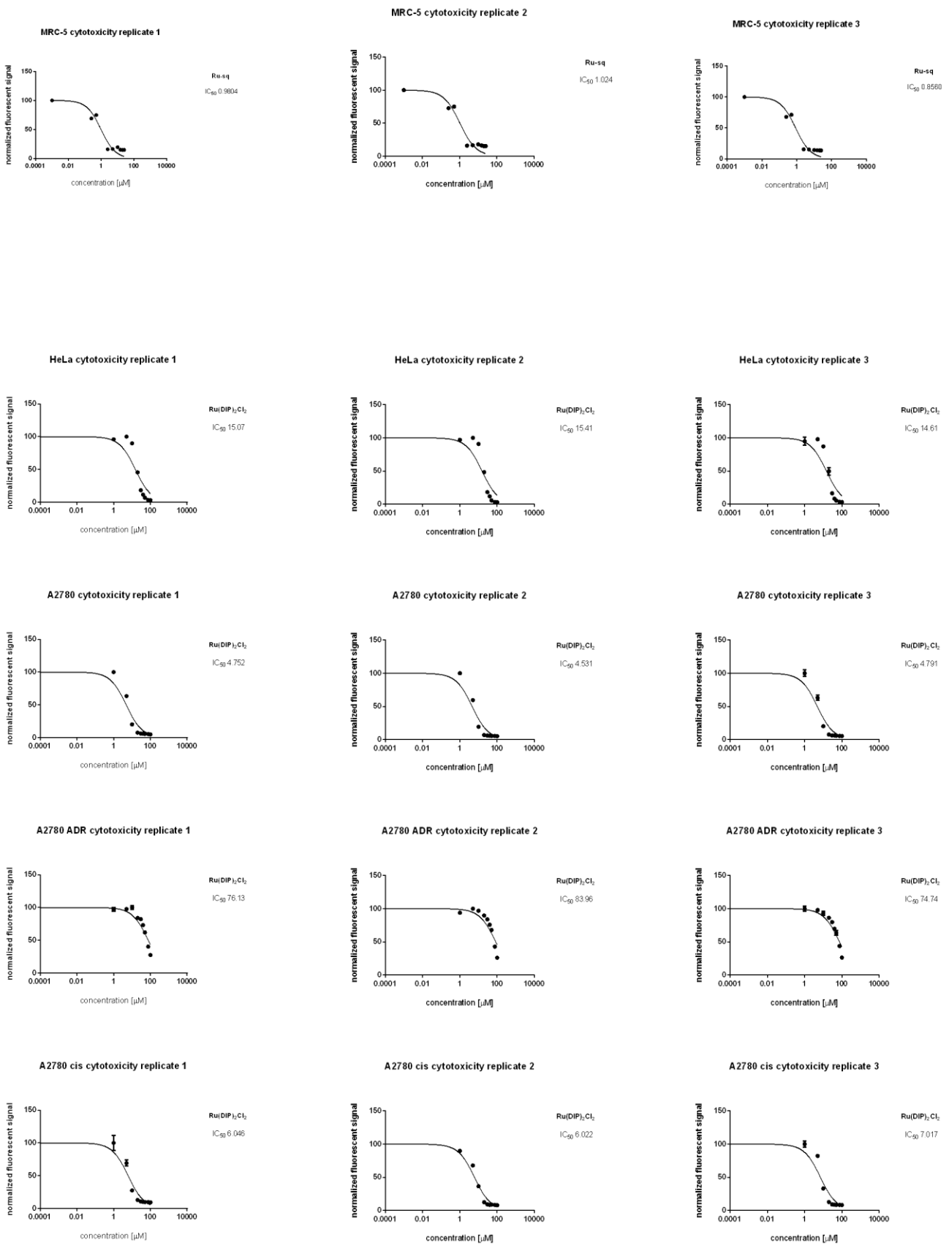


RPE-1 cytotoxicity replicate 2

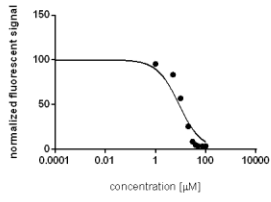


RPE-1 cytotoxicity replicate 3

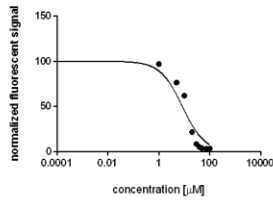




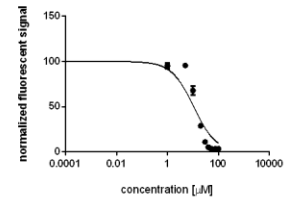
CT-26 cytotoxicity replicate 1



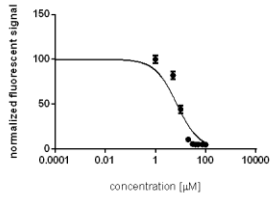
CT-26 cytotoxicity replicate 2



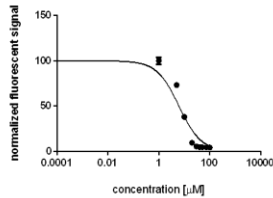
CT-26 cytotoxicity replicate 3



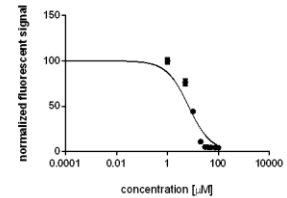
CT-26 LUC cytotoxicity replicate 1



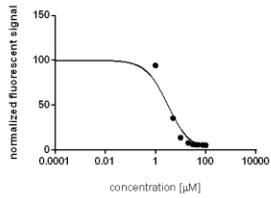
CT-26 LUC cytotoxicity replicate 2



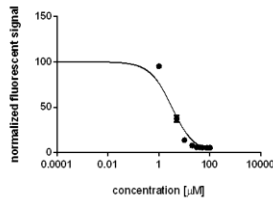
CT-26 LUC cytotoxicity replicate 3



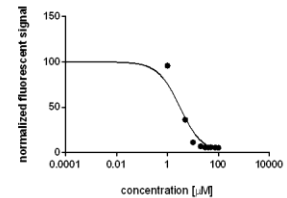
RPE-1 cytotoxicity replicate 1



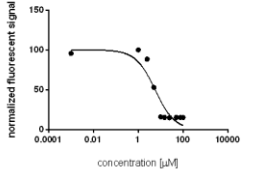
RPE-1 cytotoxicity replicate 2



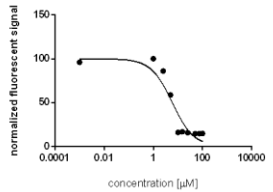
RPE-1 cytotoxicity replicate 3



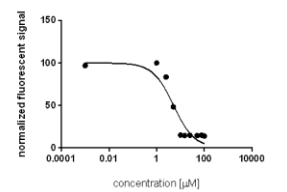
MRC-5 cytotoxicity replicate 1



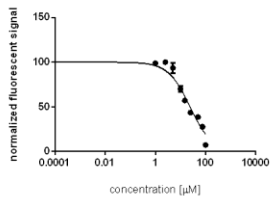
MRC-5 cytotoxicity replicate 2



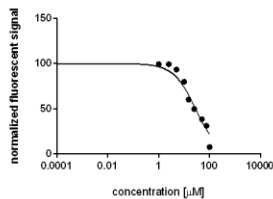
MRC-5 cytotoxicity replicate 3



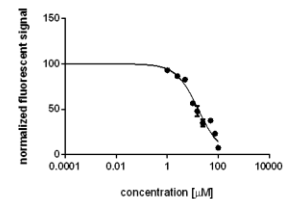
A2780 cytotoxicity replicate 1



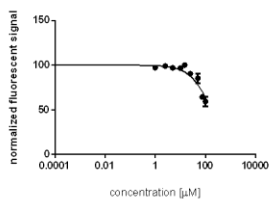
A2780 cytotoxicity replicate 2



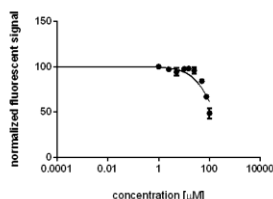
A2780 cytotoxicity replicate 3



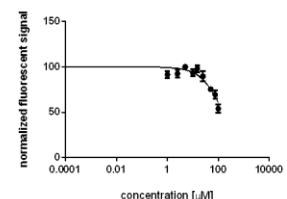
A2780 ADR cytotoxicity replicate 1



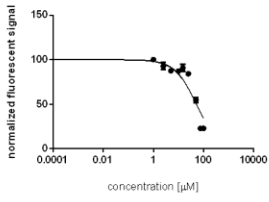
A2780 ADR cytotoxicity replicate 2



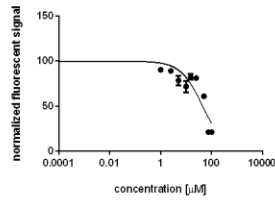
A2780 ADR cytotoxicity replicate 3



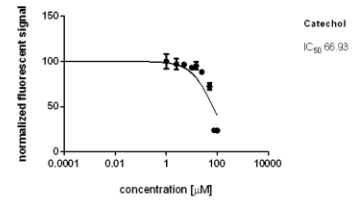
A2780 cis cytotoxicity replicate 1



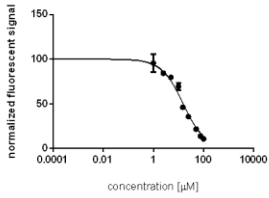
A2780 cis cytotoxicity replicate 2



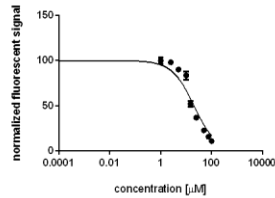
A2780 cis cytotoxicity replicate 3



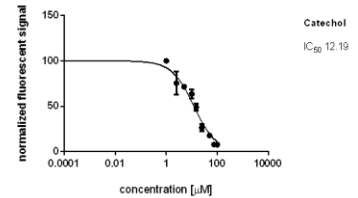
CT-26 cytotoxicity replicate 1



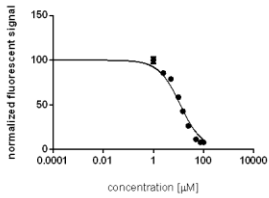
CT-26 cytotoxicity replicate 2



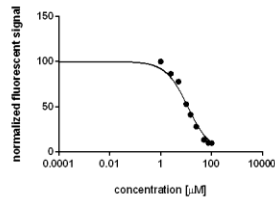
CT-26 cytotoxicity replicate 3



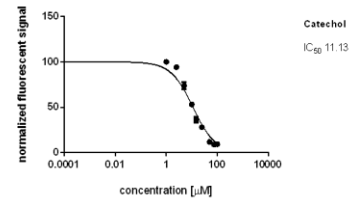
CT-26 LUC cytotoxicity replicate 1



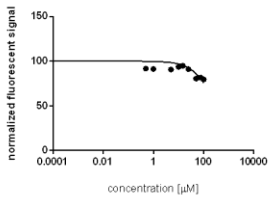
CT-26 LUC cytotoxicity replicate 2



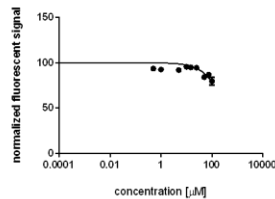
CT-26 LUC cytotoxicity replicate 3



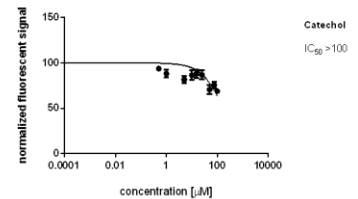
RPE-1 cytotoxicity replicate 1



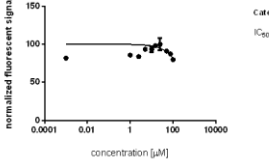
RPE-1 cytotoxicity replicate 2



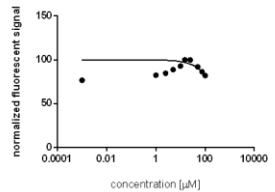
RPE-1 cytotoxicity replicate 3



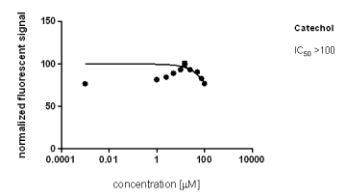
MRC-5 cytotoxicity replicate 1



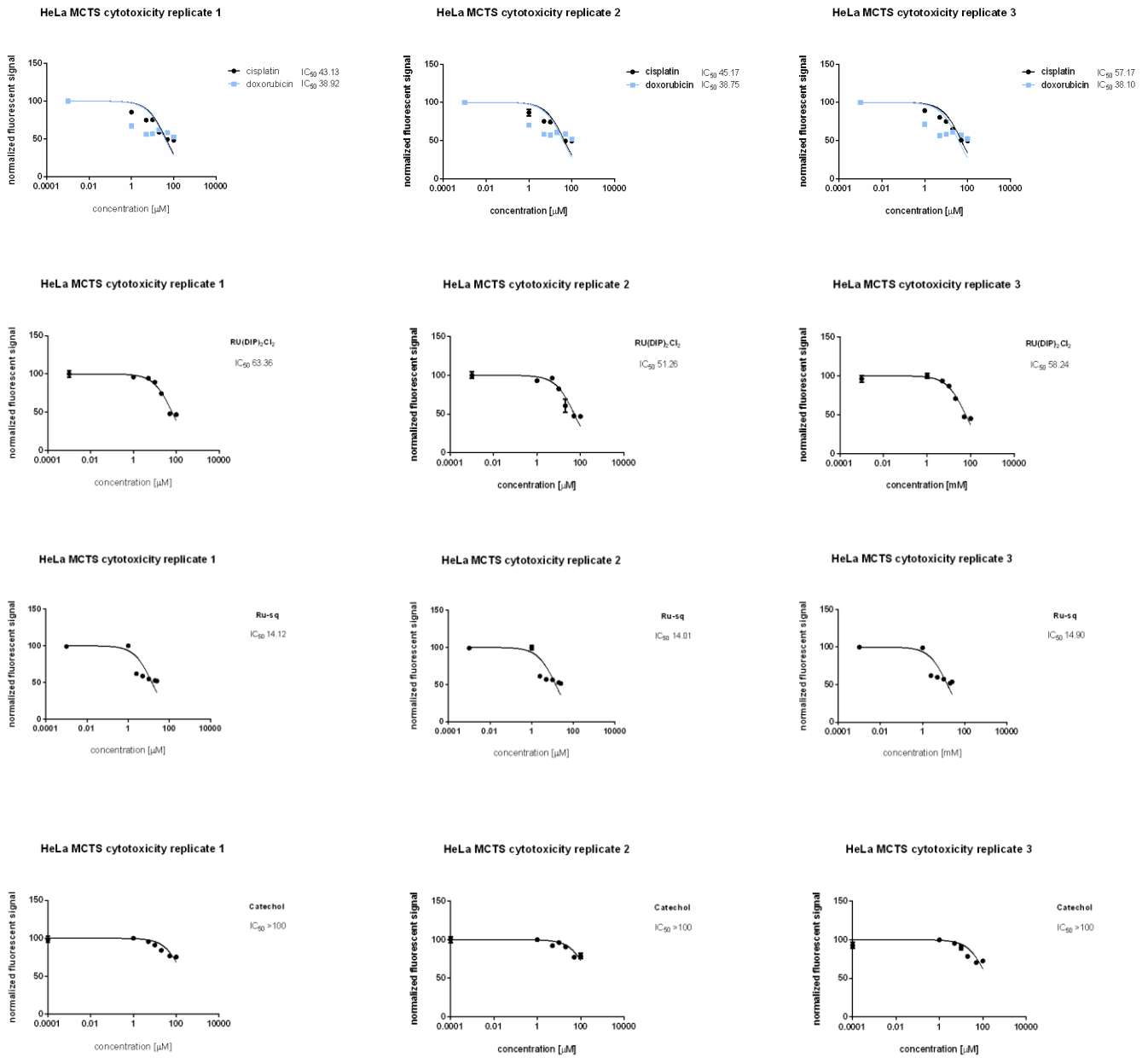
MRC-5 cytotoxicity replicate 2



MRC-5 cytotoxicity replicate 3

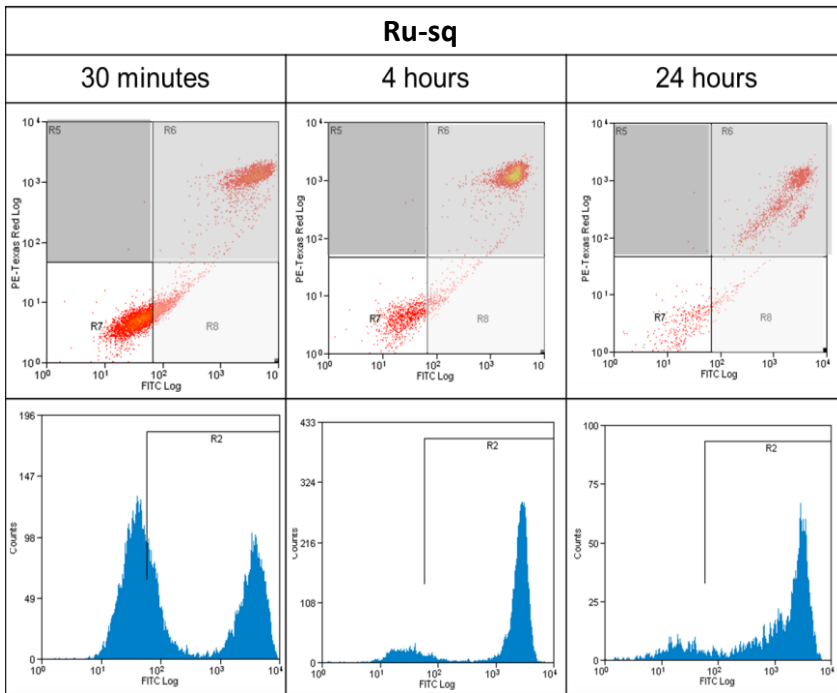


11) Figure S8. CellTiter Glo® viability Test.

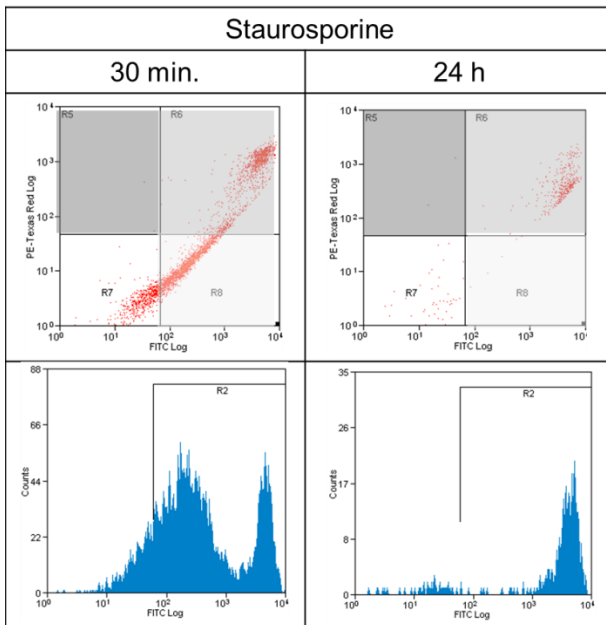


12) Figure S9. Cell Death Mechanism.

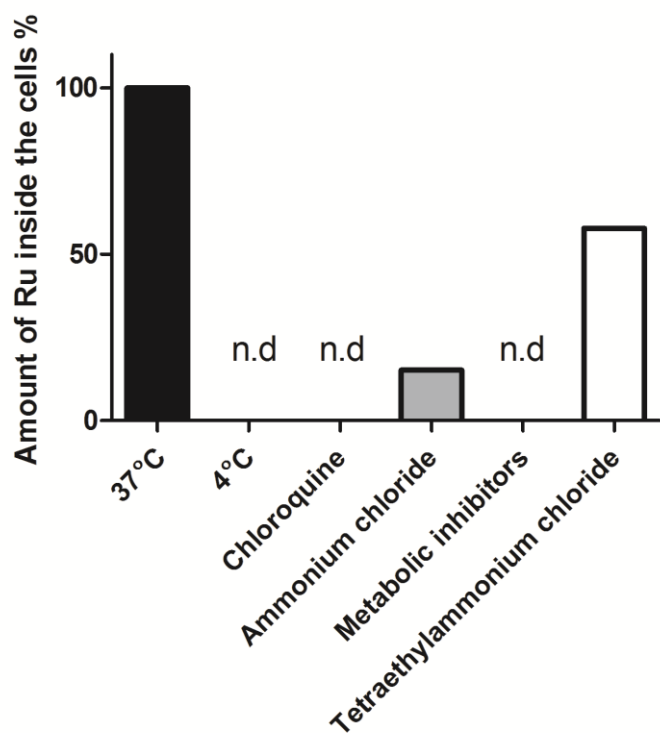
a)



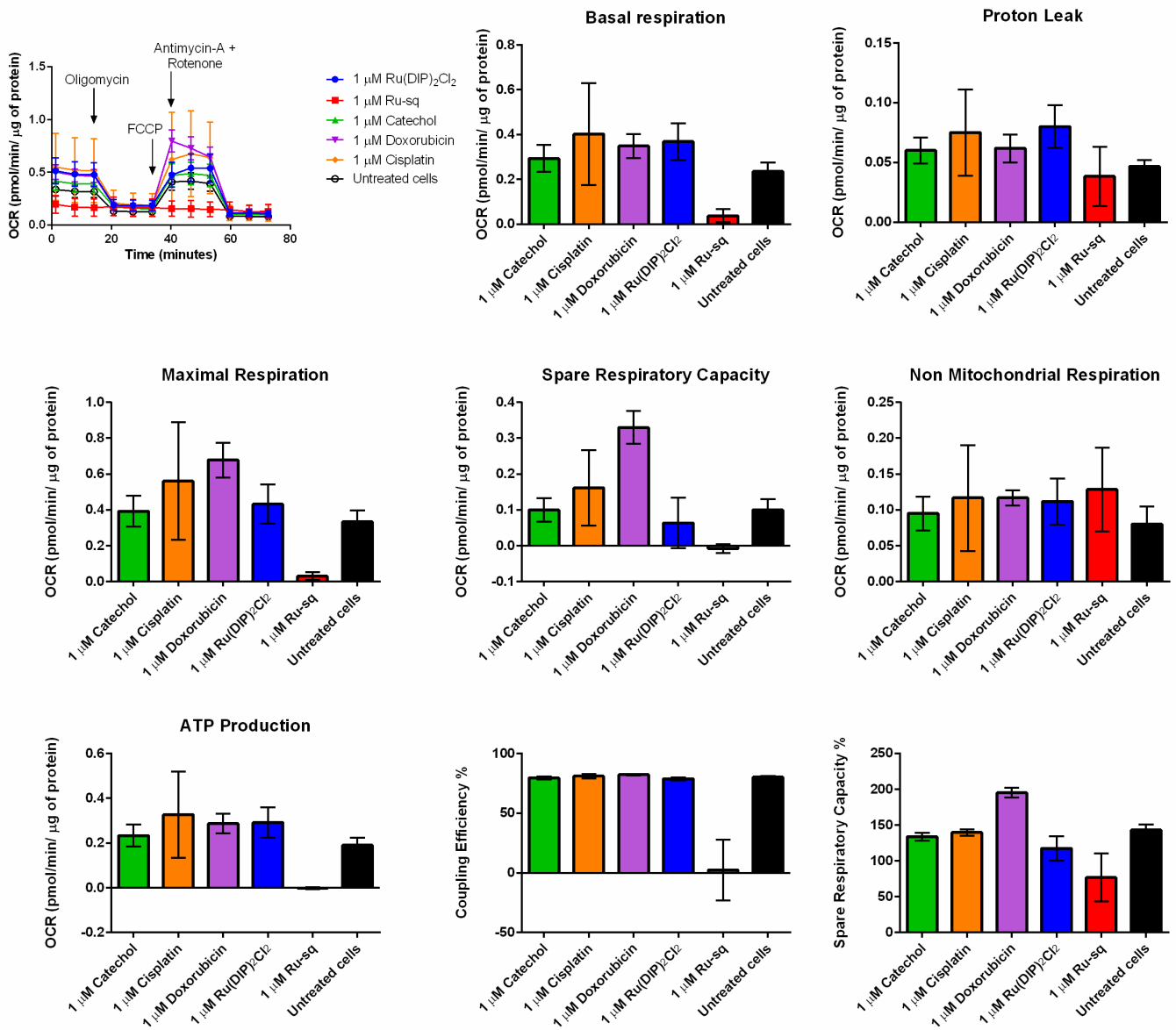
b)



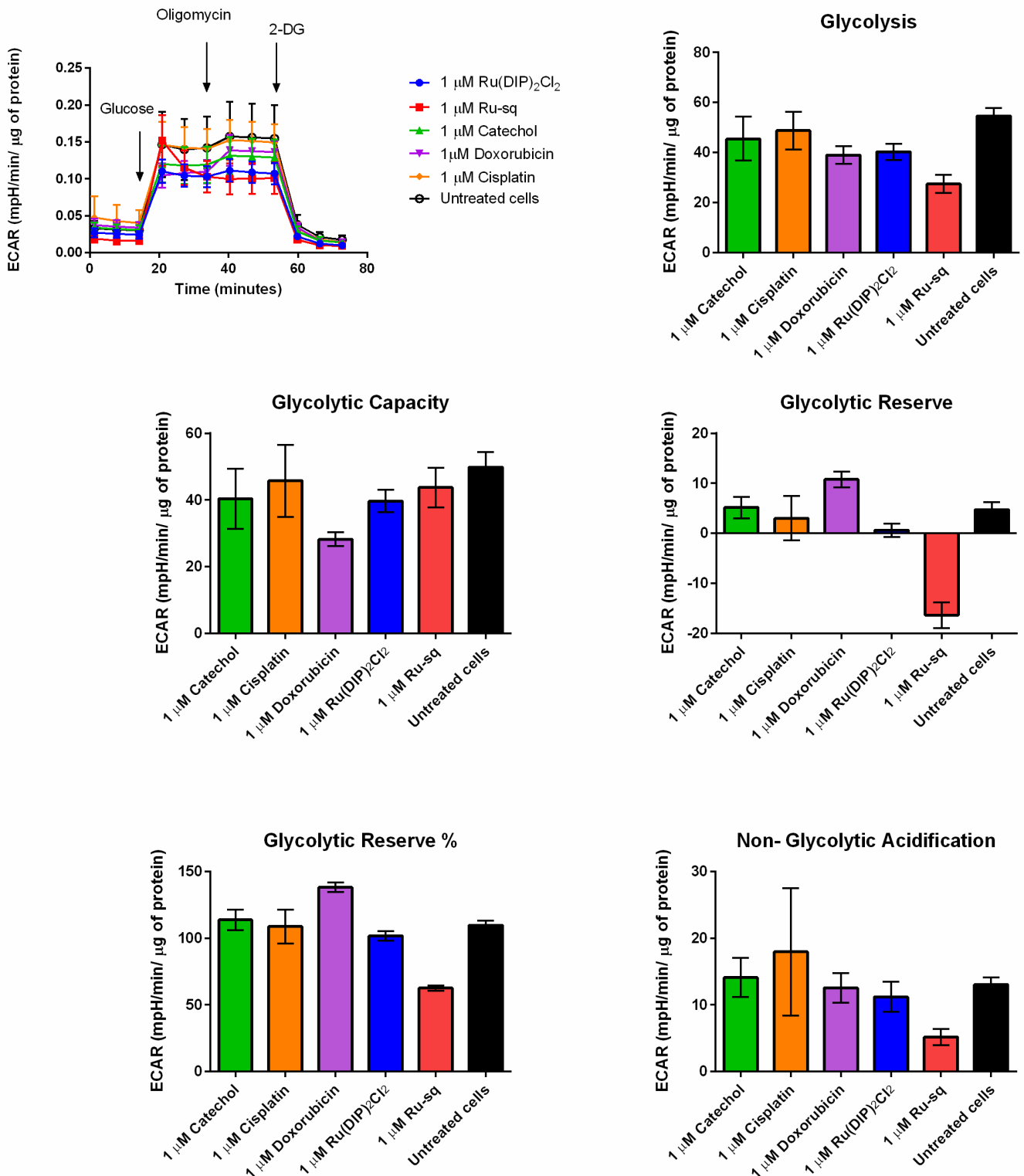
13) Figure S10. Cellular uptake mechanism of **Ru-sq**. Accumulation of ruthenium in HeLa cells in presence of different inhibitors and conditions: low temperature (4°C), blocked cellular metabolism (2-Deoxy-*D*-glucose, oligomycin), blocked endocytic pathways (chloroquine or ammonium chloride), blocked cation transporters (tetraethylammonium chloride). Cells were pre-treated with uptake inhibitors and then incubated with Ru-sq (2 h, 5 μM). Amounts of ruthenium were measured using ICP-MS. n.d-not detectable.



14) **Figure S11.** Oxygen consumption rates and different respiration parameters in HeLa cells alone or after treatment with various test compounds.



15) **Figure S12.** Extracellular acidification rate and different parameters of glycolytic respiration in HeLa cells alone or after treatment with various test compounds.



16) Figure S13. Fuel flex assay in HeLa cells. Dependency studies were performed by adding the inhibitor for the target pathway in port A and inhibitors for the other two pathways in port B while capacity studies were done using the reverse sequence. UK-5099 (20 μM), BPTES (30 μM) and etomoxir (40 μM) were used as the inhibitors for the glucose, glutamine and fatty acid pathways respectively.

